Journal of Structural Geology 32 (2010) 1212–1230

Contents lists available at ScienceDirect

Journal of Structural Geology

journal homepage: www.elsevier.com/locate/jsg

How fracture systems affect permeability development in shallow-water carbonate rocks: An example from the Gargano Peninsula, Italy

B. Larsen [a,*], I. Grunnaleite [b], A. Gudmundsson [c,1]

[a] Department of Earth Science, The University of Bergen, Allegaten 41, N-5007 Bergen, Norway
[b] International Research Institute of Stavanger, Bergen, Norway
[c] Geoscience Centre, University of Göttingen, Germany

ARTICLE INFO

Article history:
Received 10 December 2007
Received in revised
form 6 May 2009
Accepted 8 May 2009
Available online 21 May 2009

Keywords:
Fractures
Stress fields
Permeability
Carbonate rocks
Reservoirs
Numerical modelling

ABSTRACT

Fracture networks control the permeability of many reservoirs. Since the fracture patterns of petroleum reservoirs in situ are difficult to study in detail, field analogues are very important for understanding their fracture-related permeability. Here we present the results of a study of the fracture system of carbonate rocks of Lower Cretaceous age in a quarry associated with the damage zone and fault core of a major fault zone on the Gargano Peninsula in South Italy. We measured the attitude of 1541 fractures and faults along several vertical and horizontal scan lines. There are two main fracture sets: one strikes between E–W and ESE–WNW, the other NNE–SSW. A total of 675 fracture-spacing measurements indicate log-normal spacing distributions, with an arithmetic mean fracture spacing of 0.29 m and a median of 0.15 m. The data, plotted on a log–log plot, suggest three main spacing subpopulations, each of which follows approximately a power law with different fractal dimensions. Subpopulation 1, where the spacing ranges from 1 to 10 cm and the straight-line slope D ("fractal dimension") is 0.20, represents fractures confined to laminated carbonate mudstones (multilayers) that form the microbial mat deposits of a peritidal cycle. Subpopulation 2, where the spacing ranges from 11 to 55 cm and D is 0.77, represents fractures confined to thicker layers, forming a part of a peritidal cycle, the contacts of which are marked by stylolites. Subpopulation 3, where the spacing ranges from 56 to 243 cm and D is 2.81, represents fractures that dissect comparatively thick units of an entire peritidal cycle. For the spacing, the minimum coefficient of variation, C_v, defined as standard deviation divided by the mean, is 1.00 (essentially randomly spaced fractures) while its maximum C_v is 1.62, suggesting that some fractures form clusters, some clusters being denser than others. The clusters, composed of fractures with varying attitudes and therefore commonly intersecting, are likely to contribute significantly to the overall permeability of the carbonate rock. Fracture-aperture (opening) data ($N = 324$) also show a log-normal size distribution, with a mean opening of 1.01 cm and median of 0.29 cm. Log–log plots indicate that a part of this data groups into two subpopulations, I and II, each of which follows approximately a power law. The straight-line slope D ("the fractal dimension") of subpopulation I is 0.46, whereas that of subpopulation II is 1.49. We present boundary-element models showing that laminated carbonate mudstones and their contacts modify the local stress fields so as to encourage fracture offset and, commonly, arrest. Our results also show that when a fluid-driven subpopulation 2 fracture approaches subpopulation 1 fractures, the induced tensile stresses may result in the opening up of many of the subpopulation 1 fractures directly above the tip of the subpopulation 2 fractures. If, in addition, the contacts between the multilayers are weak, they also tend to open up, thus generating a large interconnected cluster of vertical fractures and horizontal contacts. The results suggest that the tensile stresses induced by a comparatively large fluid-driven subpopulation 2 fracture may contribute to the formation of an interconnected cluster of subpopulation 1 fractures and associated contacts, thereby significantly increasing the permeability of the carbonate rock.

1. Introduction

The hydromechanical properties of carbonate rocks are very variable. This is partly because carbonate rocks have different depositional patterns and, in many cases, heterogeneous fabrics.

* Corresponding author.
E-mail addresses: belinda.larsen@geo.uib.no (B. Larsen), ivar.grunnaleite@iris.no (I. Grunnaleite), a.gudmundsson@gl.rhul.ac.uk (A. Gudmundsson).
[1] Present address: Department of Earth Sciences, Queen's Building, Royal Holloway University of London, Egham TW20 0EX, UK.

0191-8141/$ – see front matter © 2009 Elsevier Ltd. All rights reserved.
doi:10.1016/j.jsg.2009.05.009

However, the variability in properties is partly due to the rocks having undergone extensive alteration after deposition which may have changed their original matrix porosity and permeability. In a subsurface reservoir with a relatively low porosity-related permeability, fractures (joints and faults) are commonly the main paths for fluid transport. Detailed studies of fracture patterns in outcropping surface analogues of such reservoirs are then needed to improve our understanding of fracture-controlled permeability in subsurface carbonate reservoirs.

Several factors control the fracture distribution in a carbonate reservoir. These factors include rock lithology and diagenesis (e.g., stylolites), mechanical properties and layering, and the current and earlier local stress fields. Stylolites are seams of clay residue that form as a result of compaction through the mechanism of pressure solution. Pressure solution, in turn, is a diffusion-related, ductile deformation mechanism where material in areas of high stress, such as surfaces orientated perpendicular to the maximum principal compressive stress, is dissolved and transported to areas of low stress, such as surfaces orientated perpendicular to the minimum principal compressive stress (Van der Pluijm and Marshak, 2004). Stylolites are most commonly found in limestones where as much as 40% of the original sequence thickness may have been dissolved through stylolitisation. In rocks with considerable clay content, the stylolites are generally wavy, whereas where the clay content is less than about 10% the stylolites become irregular sutures that appear tooth-like in cross-section (Van der Pluijm and Marshak, 2004). While many authors distinguish between stylolites and dissolution seams, the former being a serrate (tooth-like, saw-like) surface and the latter a non-serrate surface (Karcz and Scholz, 2003; Stow, 2005), here we do not make that distinction and use the term "stylolite" for both.

Fractures in layered rocks are commonly stratabound, meaning that they are confined to individual layers so that the fracture height (dip dimension) is less than or equal to the layer thickness (e.g., Bai et al., 2000). Here we refer to such a layer as a "mechanical layer". Mechanical layering has great influence on a variety of geological processes, in particular fracture propagation and arrest (Gudmundsson and Brenner, 2004; Gudmundsson, 2006). Stress rotation, for example, is common at the contacts between mechanical layers, resulting in fracture offset or arrest (Gudmundsson, 2006). Similarly, fracture spacing is often proportional to layer thickness (Price, 1966; Huang and Angelier, 1989; Narr and Suppe, 1991; Bai et al., 2000), although there are many known examples where fracture spacing in sedimentary rocks greatly differs from layer thickness (e.g., Wennberg et al., 2006; Odonne et al., 2007). By contrast, non-stratabound fractures, by definition, propagate through more than one layer and their spacing is thus not proportional to layer thickness (Odling et al., 1999).

Fracture spacing affects the mechanical properties of rocks and their permeability. The details of the processes and factors that control fracture spacing are, however, still poorly understood. There are many proposed explanations for fracture spacing (Hobbs, 1967; Gross, 1993). For example, Wu and Pollard (1995) studied the stress distribution between two adjacent fractures in a 3-layer model and varied the spacing-to-layer thickness ratio (S/T_f). They found that at a critical S/T_f value of 0.976 the stress perpendicular to the fractures changed from tensile to compressive between adjacent fractures, thereby suppressing the formation of further tensile fractures between the two. For S/T_f values lower than critical, only flaws perturbing the local stress field (or hydrofracturing) may cause the initiation of new fractures. However, Li and Yang (2007), using a similar 3-layer model, concluded that tensile stresses remain at the layer boundaries when the S/T_f ratio decreases, and these stresses can initiate fractures even though the S/T_f ratio decreases below a "critical" value.

Fracture spacing thus relates to fracture initiation, propagation and arrest, and all these factors affect the permeability of a fractured reservoir. These factors also depend on local stresses, which, in turn, are a function of the mechanical properties of the rock layers, in particular their Young's moduli and Poisson's ratios. Mechanical properties and local stresses thus control how easily fractures link to form continuous networks, which to a large extent determine the reservoir permeability. The reservoir percolation threshold is reached when a set of fractures forms an interconnected network. Whether or not this threshold is reached depends on the proportion of arrested, offset, and stratabound fractures as well as fracture attitude.

This paper has two principal aims. The first is to provide new data on fractures and how they affect the potential permeability in platform limestones of Lower Cretaceous age. For this purpose, we made detailed studies and measurements of joints and faults along several vertical and horizontal scan lines (along single stratigraphic horizons) in a working quarry with numerous, planar, wire-cut faces in south Italy (Fig. 1). Particular attention was given to the scan lines which where carefully oriented parallel to the bedding so as not to cut through several mechanical units. We focused on those fracture parameters that were most likely to affect permeability, namely attitude, spacing, arrest, and aperture. We used the statistical results to provide some general conceptual models on fracture development and fluid transport in low-permeable carbonate reservoirs. The second aim is to provide numerical models of fracture propagation and linkage in carbonate reservoirs. For this purpose, we used the boundary-element method (BEM) to study the local stresses and likely fracture paths in layered carbonate reservoirs. In these models, particular attention is paid to the effects of contacts and fine layering (laminated strata) on fracture propagation, arrest, and interconnection.

2. Geological setting

2.1. Tectonic setting

The Pizzicoli Quarry near Apricena is located in the Puglia region, southern Italy, in the western part of the Gargano Promontory (Fig. 1). The area forms the north-western part of the Apulian Platform, which is a foreland region for both the Apennines and the Dinarides–Albanides thrust and fold belts (Salvini et al., 1999). The main development of the Apennines began in the early Miocene and continued through the late Pliocene. As a result, thick Mesozoic and Cenozoic carbonate platform and deep-water basinal units overthrust the western margin of the Apulian platform in a NE direction (Bertotti et al., 2001; Brankman and Aydin, 2004; Billi et al., 2007). As a result of thrusting in a SW direction, the Dinarides formed between Eocene and early Miocene, following an older orogenesis, while the Albanides developed during the late Paleogene–middle Miocene (Bertotti et al., 2001; Billi et al., 2007).

Three major faults dissect the Gargano Promontory (Fig. 1c), namely, the E–W trending Mattinata and Rignano Faults and the WNW–ESE trending Candelaro Fault. The best studied is the Mattinata Fault with an on-land trace length of more than 40 km and a typical thickness of about 200 m (Salvini et al., 1999). The fault core is mostly 20–40 m thick, whereas the damage zone is 160–180 m or 80–90% of the total fault-zone thickness (Salvini et al., 1999). Offshore, in the Gulf of Manfredonia, the Mattinata fault joins a 130-km-long structure known as the Gondola–Grifone structural high (Patacca and Scandone, 2004).

Pull-apart basins (Pantano di Saint'Egidio) and other structures suggest that the Mattinata Fault is, partly at least, sinistral (Favali et al., 1993; Salvini et al., 1999; Billi and Salvini, 2001; Billi, 2003; Brankman and Aydin, 2004). However, some authors have argued

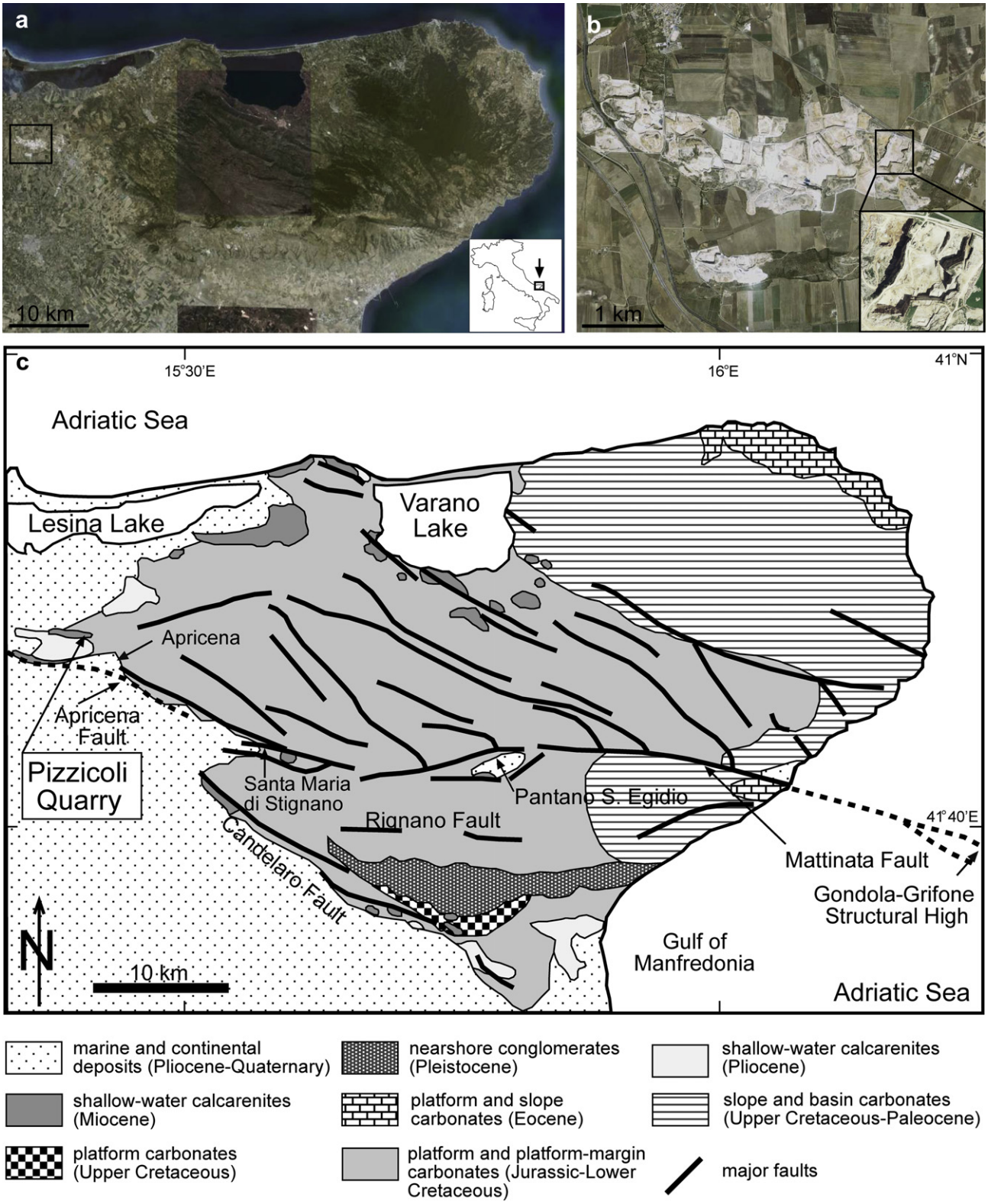

Fig. 1. (a) View of the Gargano Peninsula from Google Earth. (b) Enlargement of the square in (a) shows an E–W trending zone of quarries, where the square shows the Pizzicoli Quarry (orthophotos from Portale Cartografico Natzionale, Italy). (c) Geological map of the Gargano Peninsula (after Billi et al., 2007). The Apricena Fault and the Gondola–Grifone Structural High are taken from Patacca and Scandone (2004).

that it is primarily dextral (Doglioni et al., 1994; Anzidei et al., 1996; Morsilli and Bosellini, 1997; Bosellini et al., 1999), dextral- to sinistral inverted (de Alteriis, 1995; Gambini and Tozzi, 1996), sinistral- to dextral inverted (Chilovi et al., 2000), reverse, or a strike-slip fault with an unknown detailed sense of slip (Bosellini et al., 1993; Bertotti et al., 1999; Graziano, 1999, 2000; Casolari et al., 2000). Some of the different interpretations of the fault may be attributed to its apparent slip being partly generated as a result of

a contraction in volume by cleavage-normal rock dissolution (Nickelsen, 1972). Tondi et al. (2005) conclude that the early slip along the fault was sinistral, as indicated by the pull-apart basin and pressure solution surfaces, whereas the more recent slip is dextral, based on geomorphic and structural features, such as deflected streams.

The area is seismically active, the largest historical event being the 1627 Gargano Earthquake with a magnitude of 6.7. Its epicenter was located ~10 km southwest from Apricena, just a few kilometres east of the Apennine front (Patacca and Scandone, 2004). The 20–25-km-long fault segment (as inferred from the size of the earthquake) has, however, not been identified, whereas an E-trending, S-dipping, 30-km-long active normal fault occurs in the subsurface with a vertical throw exceeding 500 m (Patacca and Scandone, 2004). This normal fault, referred to as the Apricena Fault, joins the Mattinata Fault west of Santa Maria di Stignano, about 13 km SE from Apricena (Fig. 1).

2.2. Sedimentological setting

The Apulian Platform was a productive, isolated Bahamas-type platform during Late Jurassic–Early Cretaceous time, accumulating a 3–3.5-km-thick pile of sediments in the Gargano Promontory (Bosellini et al., 1993, 1999; Spalluto, 2004). In the western part an inner shelf environment resulted in shallow-water limestones, while slope units grade eastwards into basinal deposits, marking the transition from the Apulian Platform to the Ionian Basin (Morsilli and Bosellini, 1997). Two drowning episodes occurred during the Cretaceous, resulting in the platform becoming inactive. The first event happened during Berrisian–Valanginian time and the second during Aptian–Albian time, both of which halted carbonate production (Morsilli and Bosellini, 1997). During the Mesozoic, the platform also experienced periods of subaerial exposure, giving rise to karst and paleosol development (Bosellini, 2002). Cenozoic units are not very common in Gargano, but are found in limited areas. Eocene deposits range from marginal, slope to basinal deposits while the Miocene deposits consist of shallow-water limestones. Pliocene coastal and deltaic siliciclastics locally overlie the Cenozoic and Mesozoic carbonate deposits at the western margin of the Gargano peninsula (Fig. 1c).

2.3. Study area

The studied Pizzicoli Quarry is one of many quarries lying on an east–west ridge (Fig. 1b) that is apparently related to the damage zone of the Apricena Fault (Fig. 1). The rocks exposed in the quarry can be divided into two main units. The lower unit consists of the Lower Cretaceous rocks belonging to the San Giovanni di Rotondo Fm and is formed of a combination of strongly cemented and recrystallised wackestones and mudstone, including fenestral wackestone and algally laminated carbonate mudstones (Spalluto, 2004). These form typical shallowing-upward, peritidal cycles (Pratt et al., 1992) in 1–2-m-thick units (Fig. 2). Cycles begin with intensely bioturbated, subtidal wackestones, followed by intertidal wackestones and packstones, and culminate in supratidal fenestral and microbial mat deposits (Fig. 2b). Cycle boundaries are commonly sharp and form prominent bedding planes. Some of these are further enhanced by stylolites, while others are marked by thin (<10 cm) accumulations of red or green siliciclastic silt, interpreted as paleosols that formed during periods of exposure of the platform (Spalluto, 2004).

The top of the San Giovanni di Rotondo Fm is truncated by a regional, sub-Miocene unconformity which in the study area is marked by a well-developed palaeokarst. The surface of the Cretaceous limestones carries large- and small-scale features (rillenkarst, clints and grykes) typical of karst weathering and is associated with the extensive development of a terra rossa paleosol. Karst development postdated the main period of fracture development, as a result of which many fractures have been widened by karst-related dissolution. Terra rossa was carried down solution-widened fractures to depths of at least 15 m below the unconformity surface and some bedding planes also show solutional effects. The karstic, Lower Cretaceous limestones in the Pizzicoli Quarry are analogues to similar, oil-producing limestones in the Rospo Mare field, located 20 km offshore in the Adriatic Sea (Soudet et al., 1994). Resting unconformably on the palaeokarst surface is an approximately 9-m-thick succession of Miocene rocks. This topmost unit, often referred to as the Apricena calcarenite, consists of coarse- to fine-grained shallow-water limestones (Vartdal, 2006).

3. Fracture geometry

The fracture sets were studied on newly exposed vertical and horizontal quarry surfaces. Most of the data were collected using a profile sampling (scan line) technique (Priest, 1993) which gives a 1D spatial distribution of the fractures. Several scan lines, ~10–50 m long, from different beds and in different directions were measured with emphasis on fracture attitude, spacing and aperture. From 9 scan lines covering a total length of ~194 m, we measured 675 spacings, while the total number of measured attitudes in the quarry is 1541 and apertures 324.

Several fractures are filled with terra rossa from the Sub-Miocene unconformity or siliciclastic silts from Intra-Cretaceous paleosols, the thickness of which can be used to infer the palaeoapertures of the fractures (see Section 3.3). Many fractures, however, are vuggy, that is, have been subjected to dissolution which has increased their apertures. To measure the apertures of narrow fractures lacking fill we used a tool called "feeler gauge" (widely used for measuring gaps in internal combustion engines) whereby the smallest measurable aperture is 0.05 mm. An advantage of this tool, in addition to its high resolution, is that it allows us to measure the aperture at depth (<9 cm) inside the fracture thus avoiding the most significant effects of weathering. We also minimised the weathering effect by only considering beds in active quarry faces.

The program Statistica 7 was used to calculate the descriptive statistics, such as arithmetic mean, median and standard deviation. We tested our data for normality using normal probability plots (p-plot). A p-plot is a scatter plot where the selected variables are plotted against values expected for normal distribution (computed from Statistica). If the observed values are normally distributed, then all values should fall on a straight line. All our spacing data showed large deviations from the straight line in the p-plot, hence the spacing is not normally distributed. To get the best distribution fit, we used probability–probability plots (p–p plots) and exceedence-frequency plots (EF plots). In a p–p plot, observed values are plotted against theoretical values (Section 3.2). If the theoretical cumulative distribution closely approximates the observed distribution, then all points in this plot should fall on the diagonal line (Statsoft, 2007). All data were tested for different probability distributions. An exceedence-frequency plot is a graphical method for distinguishing between the different types of frequency distributions (Drummond and Wilkinson, 1996). Exceedence frequency, $EF(x_i)$, of a particular value x_i of the measured variable (x) is defined as the number of data (n_i) with values greater than x_i, divided by the total number of data (n) (Drummond and Wilkinson, 1996):

$$EF(x_i) = \frac{n_i(x > x_i)}{n} \quad (1)$$

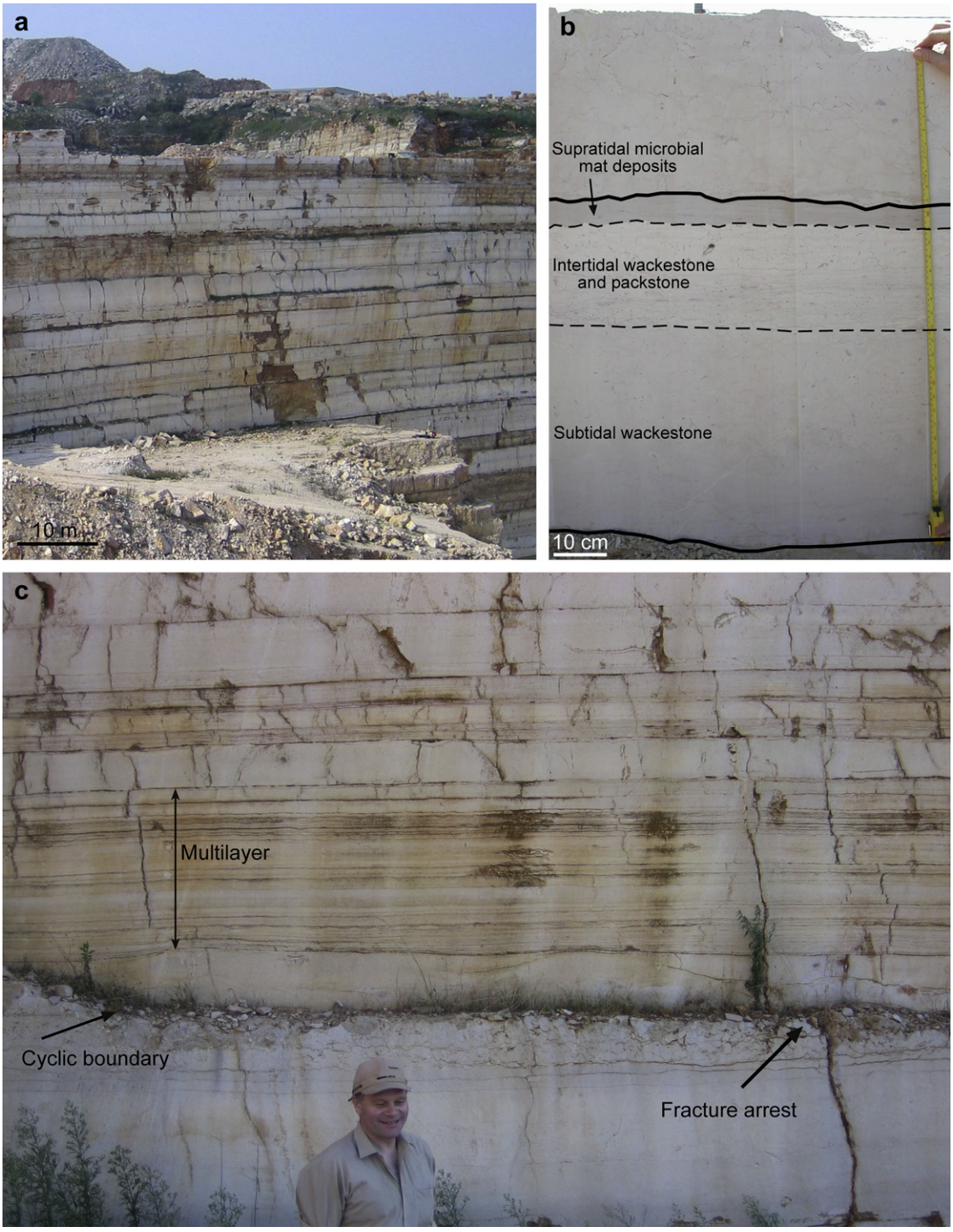

Fig. 2. (a) Peritidal cycles form mostly 1–2-m-thick units in the quarry. Cyclic boundaries are commonly sharp and form prominent bedding planes. (b) One 63-cm-cycle unit: bioturbated, subtidal wackestone at the bottom, followed by intertidal wackestone and packstone, and culminate in supratidal fenestral and microbial mat deposits. (c) Cyclic boundary marked by the accumulation of red siliciclastic silt. Many fractures arrest or offset at the cyclic boundaries. Note the (laminated) multilayer above the boundary; fractures are offset at many of the contacts, indicating a high material toughness and that the fractures have difficulties propagating through the multilayer.

Another measure of fracture spacing is the coefficient of variation, C_v, defined as the standard deviation divided by the mean (Cox and Lewis, 1966); it gives the degree of clustering along a scan line (Gillespie et al., 1999). If the standard deviation equals the mean, such as in the case of a negative exponential distribution, then $C_v = 1$ and the spacing of fractures is random. If, however, the standard deviation is higher than the mean, so that $C_v > 1$, the fractures are clustered; in contrast, for $C_v < 1$ the fractures are roughly evenly spaced (Gillespie et al., 1999; Odling et al., 1999). Finally, if the standard deviation is zero, then $C_v = 0$ and the fractures are perfectly evenly spaced.

At first glance fracture geometries in Pizzicoli Quarry seem to be rather irregular, for example as regards attitude (Fig. 3a). Analysis of the data, however, shows that they form several comparatively

regular systems. Mechanically, most of the fractures are extension fractures, that is, joints, but some are shear fractures, that is faults, most of which have displacements of less than 0.5 m (Fig. 3b). Some of the faults contain breccia with slickenlines in their cores. Only three comparatively large faults are exposed in the quarry. Two of these faults strike NNE and one NW. The NW-striking fault has a displacement of ~15 m and predates the Miocene rocks (Fig. 3c), while the two NNE-striking faults have displacements of ~2.5 m.

3.1. Attitude

We measured 853 fracture attitudes (strike and dip) on vertical walls, while 688 fracture strikes were measured on subhorizontal bedding planes. Most of the fractures dip from steeply inclined to vertical, whereas there are two main strike directions (Fig. 4). The dominant strike direction is between E–W and ESE–WNW and it occurs throughout the quarry. The second main strike direction is NNE–SSW, a direction which is common in scan line G-7 in the upper part of the quarry.

3.2. Spacing

Spacing is defined as the distance between fractures measured along a scan line, while the fracture frequency is the number of fractures per unit length along a scan line (Priest, 1993). Spacing is thus the inverse of fracture frequency. A total number of 675 spacing measurements made along the 9 scan lines are presented as histograms in Fig. 5. The descriptive statistics for each scan line, such as arithmetic mean, median, standard deviation and coefficient of variation, C_v, are given in Table 1. The mean spacing is 0.29 m, the median spacing is 0.15 m and the standard deviation is 0.34 m. The calculated C_v values from the 9 scan lines range between 1.00 and 1.62. This means that the fractures are generally clustered, some clusters being denser than others (Table 1).

The spacing is characterised by a crude log-normal distribution (Fig. 6). However, the probability–probability plots from scan lines number G-4, G-5_2a and G-5_2b show some deviations from a log-normal distribution (Fig. 6). One explanation is that the deviations are caused by a sampling bias; these three scan lines are the shortest and therefore have comparatively few spacing measurements. The exceedence-frequency plots of all spacing measurements are approximately linear on a plot with a log-scale *x*-axis (spacing) and a probability scale *y*-axis (frequency) (Fig. 7). A straight line in such a plot indicates a log-normal distribution, but with some artefacts. These artefacts can be partly due to the sampling bias, and partly to a truncation bias on the smallest spacing measurements. Some 37.5% of the spacing measurements are between 1 and 10 cm, 45.2% between 11 and 55 cm, and 16% between 56 and 247 cm (Fig. 7). The maximum spacing observed in the quarry is 247 cm, but the maximum spacing value extrapolated from the straight line is 400 cm (Fig. 7).

While log-normal distributions of fracture spacings have been obtained by many authors (e.g., Narr and Suppe, 1991; Rives et al., 1992; Becker and Gross, 1996; Gillespie et al., 2001), other

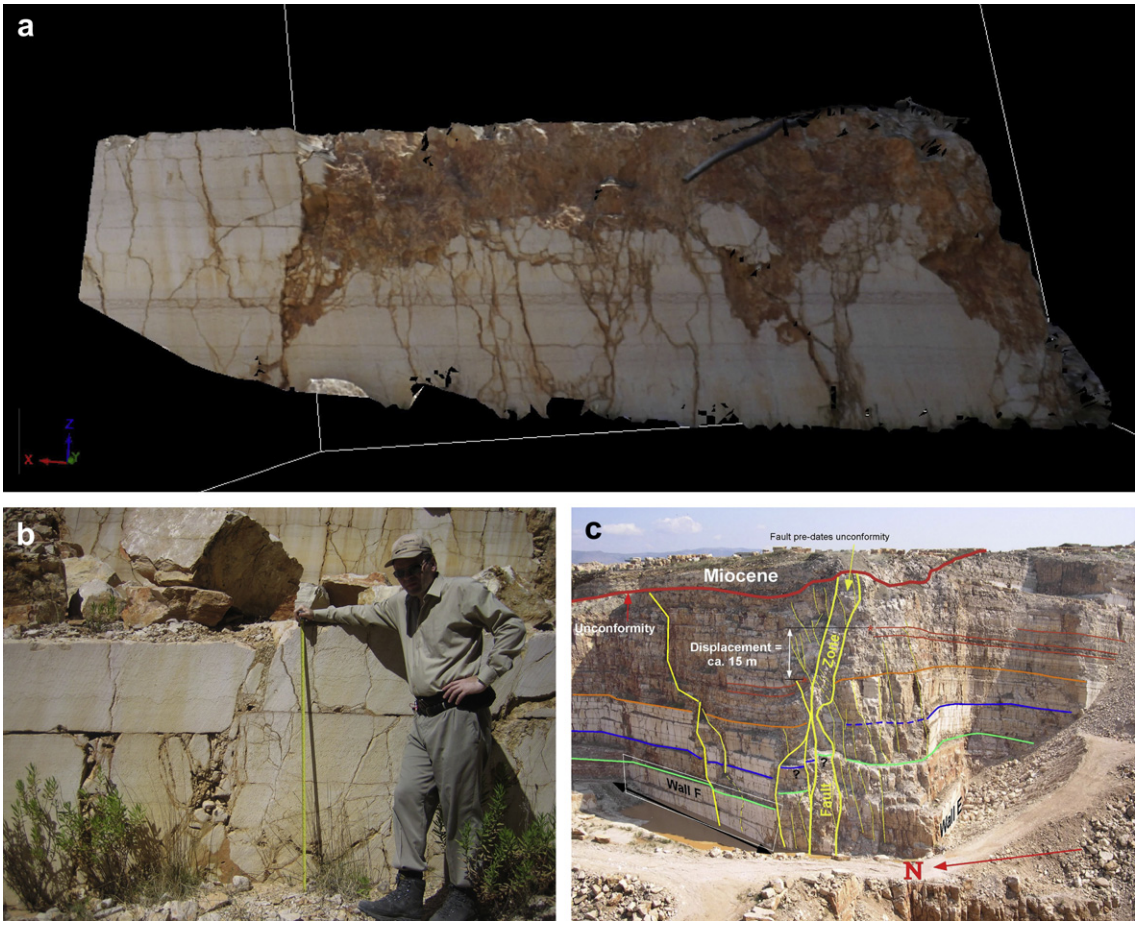

Fig. 3. Fractures in the Pizzicoli Quarry. (a) A typical quarry wall; the length of wall is 10 m and view is WNW. (b) View NNW, a brecciated fault with displacement of about 10 cm. (c) View E, a fault zone with a vertical displacement of about 15 m.

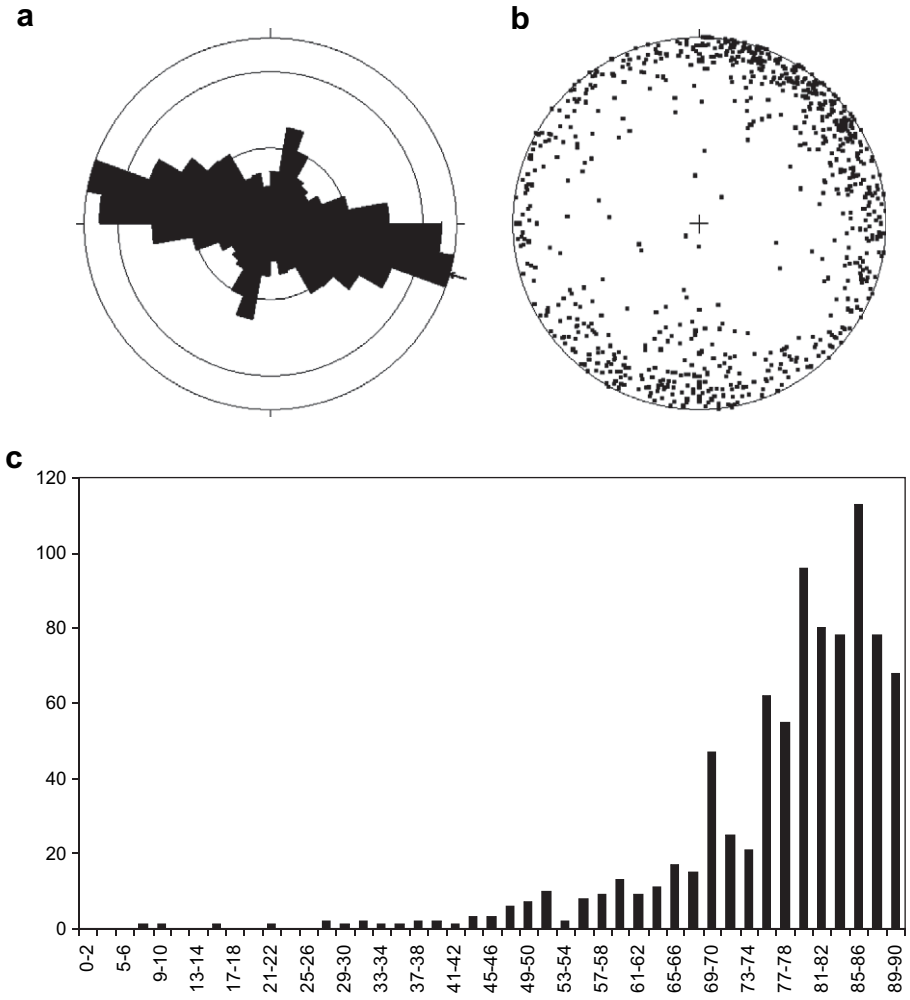

Fig. 4. (a) Rose diagram of fracture attitude measured in Lower Cretaceous rocks exposed in the Pizzicoli Quarry. Most fractures strike W to WNW (mean direction is 106–286). Sector angle is 10° and circle interval is 5%. $N = 1541$. (b) Stereoplot of 853 fractures exposed in vertical walls. (c) Histogram of fracture dip indicate that most fractures are sub-vertical to vertical ($N = 853$).

distributions have been obtained as well (Rives et al., 1992). Some authors suggest that spacing distribution changes with the evolution of the fracture set. For example, Rives et al. (1992) found that during the evolution of a joint system, joint spacing started as a negative exponential distribution (clustered fractures), then evolved into a log-normal distribution (infilling of new joints), and ended as a normal distribution (increased infilling of joints gives a constant spacing). Constant spacing may also evolve because of stress shadows around fractures that inhibit the development of new fractures, resulting in fracture saturation (Bai et al., 2000). However, different fracture-spacing distributions may also rise from sampling bias (Ortega et al., 2006).

To test whether or not our spacing data are fractal (meaning that the distribution fits a power law), we plotted the logarithmic values of frequency and spacing in an exceedence-frequency diagram (Fig. 8). The graph can be approximated by three straight lines indicating that our data consist of three spacing subpopulations. Subpopulation 1 has a spacing of 1–10 cm, a goodness-of-fit coefficient $R^2 = 0.9057$, and a straight-line slope ("fractal dimension") $D = 0.20$. Subpopulation 2 has a spacing of 11–55 cm, $R^2 = 0.9910$, and $D = 0.77$. Subpopulation 3 has a spacing of 56–243 cm, $R^2 = 0.9775$, and $D = 2.81$ (Fig. 8).

The observed peritidal cycles in the quarry are mainly represented by 1–2-m-thick units. However, some cycles are larger, while others are smaller; for example, the thickness of the complete cycle in Fig. 2b is 63 cm. Many fractures are arrested or offset at boundaries between parts of, or entire, peritidal cycles. Our data suggest that the three spacing subpopulations (Fig. 8) show some relation to these boundaries, but the only one with a clear relation between thickness and spacing is subpopulation 3. More specifically, subpopulation 3 represents fractures that span an entire peritidal cycle, so that the fracture spacing is equal to the cycle thickness or fracture height (dip dimension). Most of the fractures in subpopulation 3 are sub-vertical and do not propagate through the cyclic boundaries. They are thus unlikely to connect to subpopulation 3 fractures in the adjacent cycles, except when there are subpopulation 2 and 1 fractures in between to connect them. This means that for subpopulation 3 fractures to contribute to the permeability of the rock, their nearby tips must be connected through smaller fractures, namely fractures of subpopulation 2 or 1.

Subpopulation 2, with spacings of 11–55 cm, contains 45.2% of the total. In our interpretation, subpopulation 2 represents fractures which are controlled by boundaries between parts of, rather than entire, peritidal cycles. Many of these boundaries in between the whole cycles are stylolites, and these are commonly observed to arrest fractures. It follows that many stylolites function as mechanical boundaries inside peritidal cycles, and that the fractures of subpopulation 2 do not extend through the thickness (mechanical

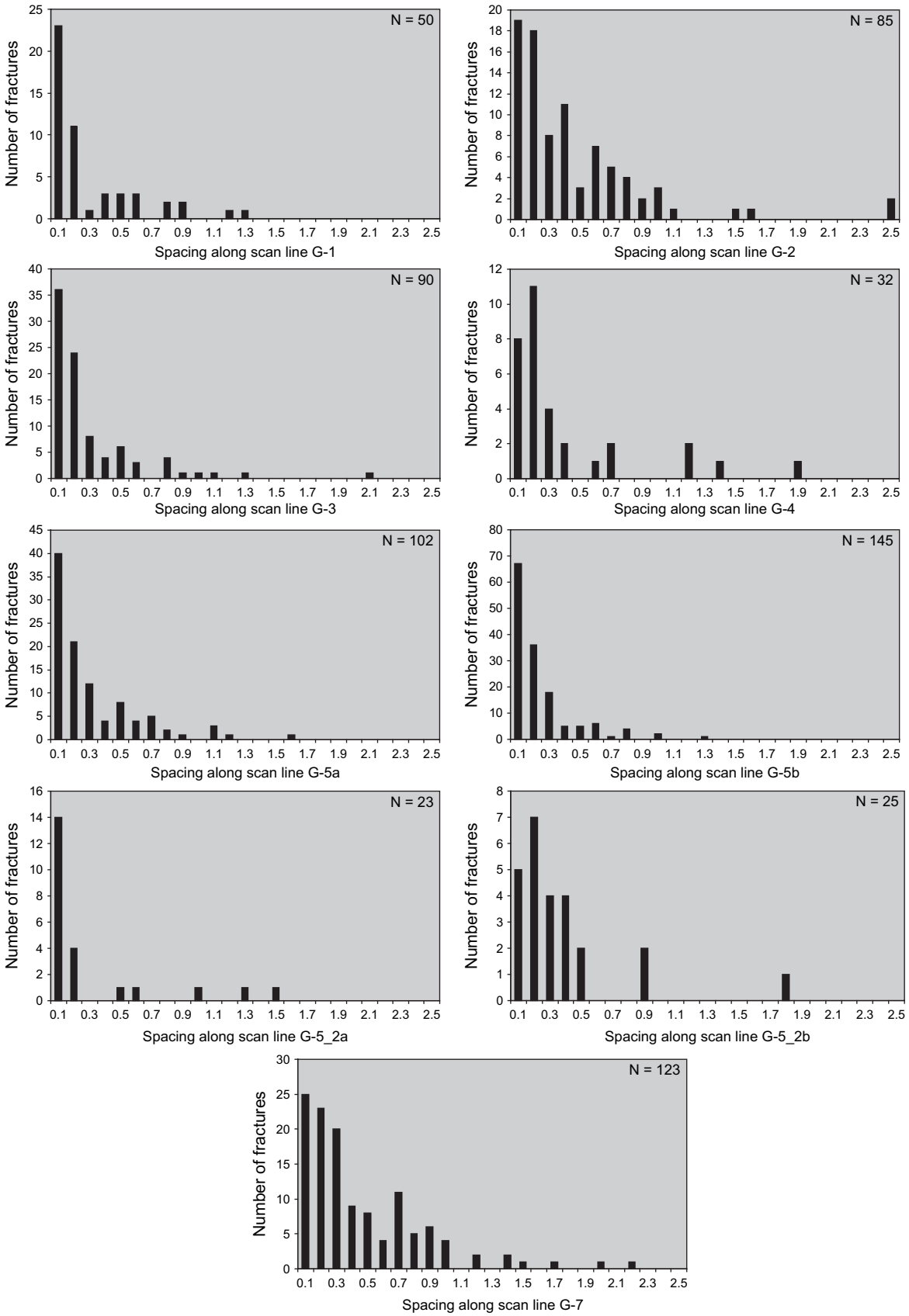

Fig. 5. Fracture spacings along 9 scan lines measured in the rocks of the Pizzicoli Quarry. The total number of measured spacings is $N = 675$.

Table 1
Descriptive statistics. (a) All fracture-spacing measurements. (b) Spacings between open fractures.

Scan line	Scan line orientation	*N* spacing	Scan line length	Mean spacing	Median spacing	Standard deviation	Minimum spacing	Maximum spacing	C_v
(a)									
G-1	SE–NW	50	12.1 m	0.24 m	0.11 m	0.30 m	0.001 m	1.22 m	1.25
G-2	ENE–WSW	85	34.3 m	0.40 m	0.25 m	0.45 m	0.02 m	2.47 m	1.13
G-3	ENE–WSW	90	21.8 m	0.24 m	0.13 m	0.32 m	0.001 m	2.10 m	1.33
G-4	ENE–WSW	32	11.2 m	0.35 m	0.15 m	0.44 m	0.02 m	1.83 m	1.27
G-5a	NNE–SSW	102	26.0 m	0.25 m	0.13 m	0.29 m	0.001 m	1.54 m	1.15
G-5b	NNE–SSW	145	26.0 m	0.18 m	0.10 m	0.21 m	0.01 m	1.20 m	1.18
G-5_2a	NE–SW	23	6.4 m	0.25 m	0.06 m	0.40 m	0.02 m	1.43 m	1.62
G-5_2b	NE–SW	25	6.4 m	0.28 m	0.20 m	0.29 m	0.01 m	1.17 m	1.02
G-7	E–W	123	50.0 m	0.40 m	0.25 m	0.40 m	0.01 m	2.12 m	1.00
(b)									
G-1	SE–NW	17	12.1 m	0.70 m	0.48 m	0.72 m	0.02 m	2.06 m	1.03
G-2	ENE–WSW	41	34.3 m	0.83 m	0.73 m	0.78 m	0.02 m	3.53 m	0.94
G-3	ENE–WSW	20	21.8 m	0.98 m	0.48 m	1.25 m	0.04 m	4.18 m	1.28
G-4	ENE–WSW	12	11.2 m	0.90 m	0.23 m	0.98 m	0.02 m	2.55 m	1.09
G-5a	NNE–SSW	32	26.0 m	0.78 m	0.59 m	0.82 m	0.001 m	4.19 m	1.04
G-5b	NNE–SSW	37	26.0 m	0.66 m	0.46 m	0.82 m	0.03 m	3.98 m	1.24
G-5_2a	NE–SW	6	6.4 m	0.89 m	0.96 m	0.75 m	0.05 m	1.81 m	0.84
G-5_2b	NE–SW	6	6.4 m	0.68 m	0.31 m	0.74 m	0.17 m	2.08 m	1.09
G-7	E–W	75	50.0 m	0.65 m	0.35 m	0.89 m	0.01 m	4.93 m	1.36

layer) of an entire cycle. Nevertheless, the close spacing and different attitudes of the subpopulation 2 fractures suggest that many of them are interconnected and therefore, when also connected to subpopulation 3 fractures, likely to greatly contribute to the overall permeability of the rock.

Some of the fractures belonging to subpopulation 1, with a spacing of 1–10 cm, are hosted by laminated carbonate mudstone (Fig. 9). In our interpretation, these fractures contribute to permeability primarily through linking the larger fractures of subpopulation 2, thereby forming interconnected fracture networks.

One conclusion of our studies is that we do not find any clear general relationship between fracture spacing and bed thickness. While such a relationship apparently exists for fractures in subpopulation 3, the relationship is unclear or nonexisting for fractures in subpopulations 2 and 1. One reason is that the stylolites function as mechanical boundaries to such an extent that there are commonly several mechanical layers inside a single peritidal cycle. These mechanical layers vary laterally and are not continuous. Fractures belonging to subpopulation 1 and 2 indicate that these mechanical layers vary in thickness between 1 and 55 cm, while for subpopulation 3 the peritidal cycles function as mechanical layers where fracture spacing is crudely related to bed thickness.

3.3. Aperture

An idealised fracture consists of two parallel surfaces and its aperture is defined as the distance perpendicular to the two surfaces. A natural fracture usually has non-smooth surfaces such that the distance is not constant. Some authors use the term "opening" for natural fractures and "aperture" for fractures when focusing on mechanical characteristics (Bai and Pollard, 2001). The term kinematic aperture refers to the total width of the fracture opening, including mineral fill and siliciclastic silts, so that the open part of the fracture is generally less than its kinematic aperture (Laubach and Gale, 2006). In this paper, when discussing aperture we mean the kinematic aperture.

We measured a total of 324 apertures (Fig. 10), the mean being 1.01 cm, the median 0.29 cm, and the standard deviation of 1.84 cm. The coefficient of variation, C_v, is 1.82. The measured apertures represent the average aperture of each fracture. Even though we did not measure fracture apertures clearly affected by dissolution, some of the largest apertures we measured could be somewhat affected by dissolution; the median, therefore, better represents common fracture apertures.

An exceedence-frequency plot is used to visualize the aperture-size distributions (Fig. 11). When the *x*-axis is a logarithmic scale (aperture) and the *y*-axis a probability scale (frequency), the data plots as a straight line, indicating a log-normal distribution of aperture data. The largest measured aperture is 15 cm, but the maximum aperture extrapolated from the straight line is 25 cm (Fig. 11). A maximum value of 25 cm seems rather large and it may indicate, again, that some of the larger measured apertures are affected by dissolution. When the aperture and frequency are plotted as logarithmic values on an exceedence-frequency diagram, the graphs approximate two straight lines, indicating a bimodal fractal data set (Fig. 12). Subpopulation I has an aperture range of 0.07–1.0 cm, $R^2 = 0.9840$, and $D = 0.46$. Subpopulation II has an aperture range of 1.1–10.0 cm, $R^2 = 0.9679$, and $D = 1.49$.

3.4. Spacing versus aperture

254 of the total of 324 measured apertures were measured along the 9 scan lines (Fig. 13). The spacing between open fractures along the 9 scan lines described earlier yield a total of 245 spacing measurements. The values from each scan line are given in Table 1b. The mean spacing is 0.79 m, the median 0.51 m, and the standard deviation 0.86. The coefficient of variation, C_v, is between 0.84 and 1.36 (Table 1b).

When comparing all the fractures (both open and closed) with open fractures (those with measured apertures) there are some differences in the calculated coefficient of variation, C_v. These differences may indicate that the open fractures are more randomly distributed than the fractures in general (open and closed). The average C_v for open fractures is 1.10 whereas that for all the fractures is 1.22, suggesting that the open fractures are more evenly distributed than the fractures in general. More specifically, for six of the nine scan lines, C_v is smaller for the open fractures (than for open and closed), while for three scan lines C_v is higher for the open fractures (Table 1b). One possible explanation is that the more clustered fractures were faults (shear fractures), whereas the more evenly distributed fractures were pure extension fractures (joints). However, we found no evidence for such a mechanical difference.

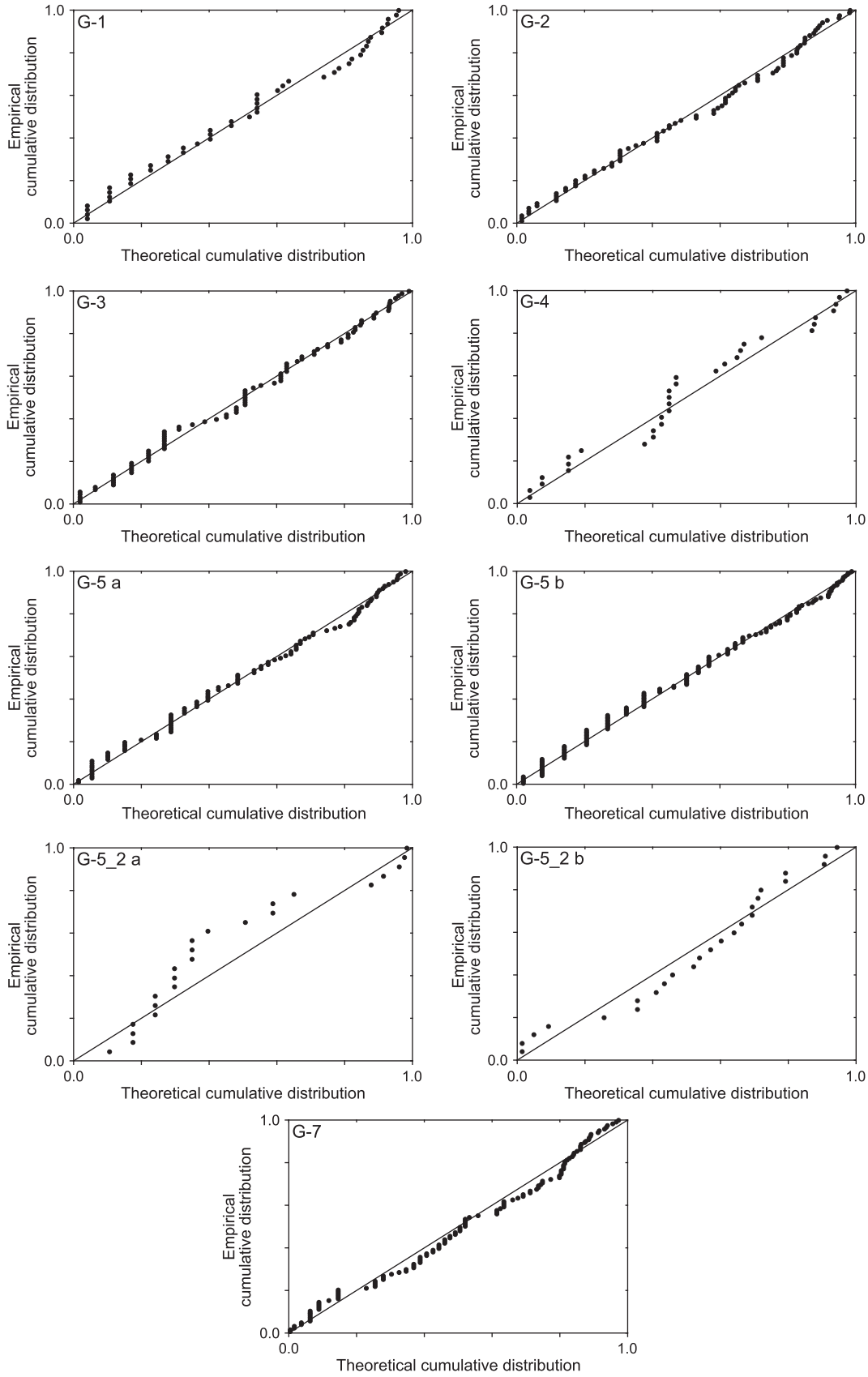

Fig. 6. Probability–probability plots showing generally log-normal fracture-spacing distributions. The main deviations occur in scan line G-4, G-5_2a and G-5_2b.

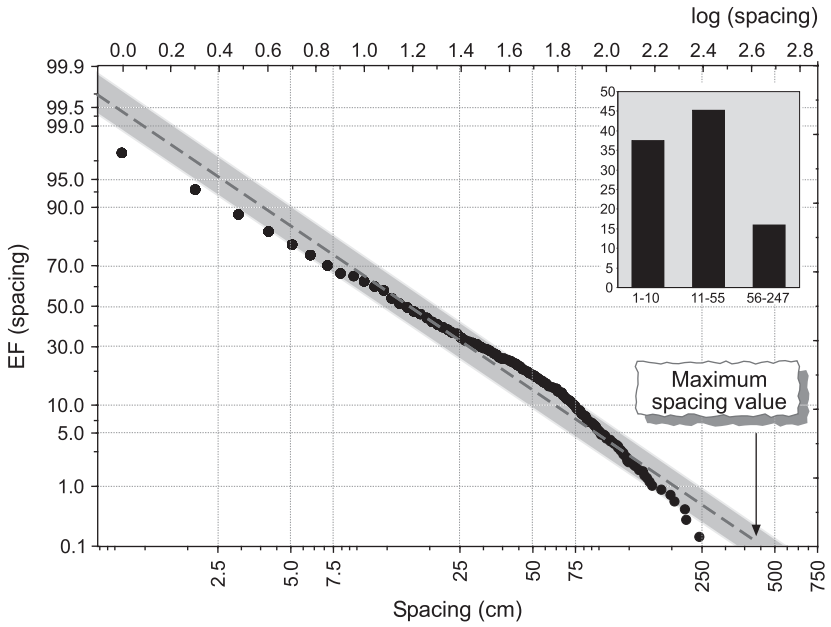

Fig. 7. Exceedence-frequency plot of all fracture-spacing measurements with the spacing on a logarithmic scale and the frequency on a probability scale. The plot can be approximated as a straight line, indicating a general log-normal distribution (with some artefacts). The extrapolated, broken straight line (lower right of the figure) gives the estimated maximum spacing. The inset diagram shows the class limits and the frequency (%) of fracture spacings in the three main subpopulations.

4. Numerical modelling

Fracture attitude, spacing, offset and arrest all greatly affect the potential permeability in a reservoir. Our results show that many fractures are offset or arrested at contacts between mechanical layers and that there are comparatively few large faults in the quarry (Fig. 3c). Thus, while the faults are likely to be the main conductors of fluids for a reservoir composed of the quarry rocks, it is clear that, since the large faults are so few, interconnected clusters of joints and other small-scale fractures would probably greatly contribute to fluid transport. However, as discussed earlier, many fracture sets do not form interconnected clusters because so many of the fractures become arrested at contacts between mechanical layers, that is, they become stratabound.

For a better understanding of the conditions under which existing fractures in different layers would tend to form interconnected clusters, and thereby reach the percolation threshold (Stauffer and Aharony, 1994), we constructed several boundary-element models.

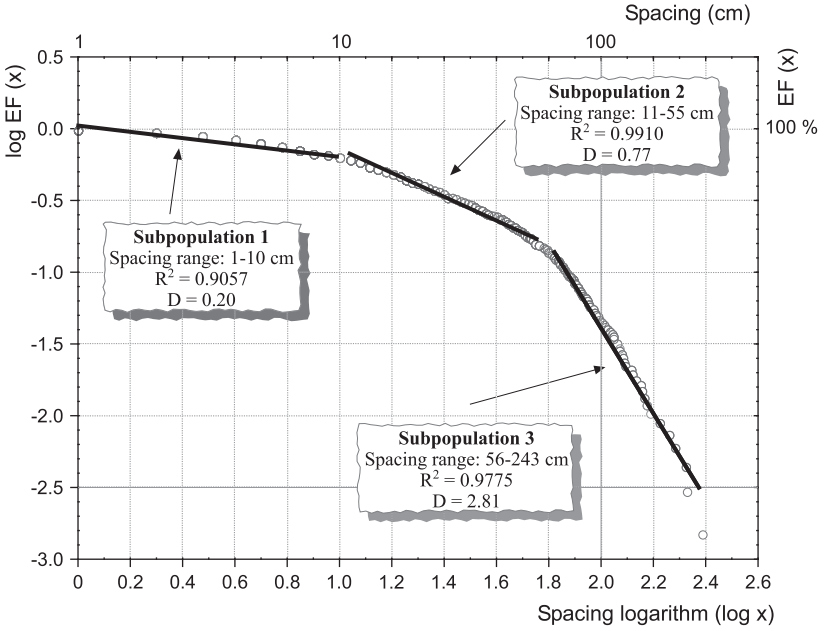

Fig. 8. Exceedence-frequency plot of the fracture-spacing data set, with both frequency and spacing on logarithmic scales. The graph can be approximated by three straight lines, with different dips, indicating three spacing subpopulations that are roughly power laws with different straight-line slopes D ("fractal dimensions"). The highest value in subpopulation 3 is here 243 (rather than 247) because when calculating the exceedence frequency the highest number (247) is given the value zero.

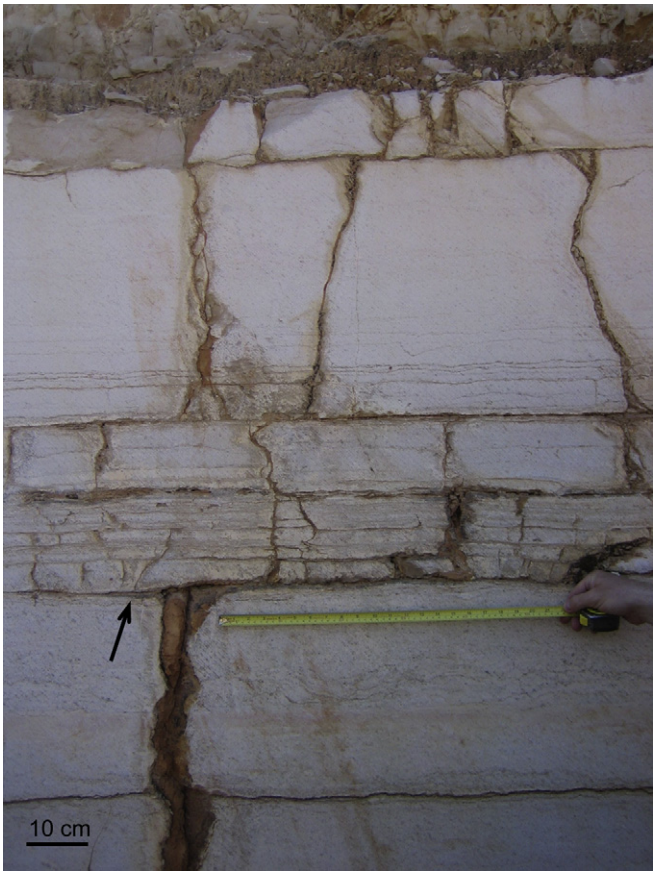

Fig. 9. Fractures from subpopulation 1 located in microbial mat deposits. View NW.

To make the models as realistic as possible, we selected field examples of fractures (Fig. 14) and modelled their geometric arrangement as accurately as possible (Fig. 15).

In the present model (Fig. 15), we are interested in knowing how a fluid-driven fracture (a hydrofracture) propagating vertically towards the existing fracture systems in the layers above would affect the fractures. In particular, we want to test the likelihood of the fractures linking up into a permeable cluster. Thus, we are not modelling the sizes of the fracture apertures (the opening displacements), but rather whether the discontinuities in a certain rock volume would tend to link up into a cluster for the given boundary conditions. The fact that many fracture apertures show the effect of dissolution (Fig. 9) is of no concern in the present numerical model. To avoid rigid-body translation or rotation, all the models are fastened in their corners, using the condition of no displacement (indicated by crosses in Figs. 15–17).

The model was thus run with the fluid overpressure (fluid pressure in excess of the horizontal compressive stress normal to the fracture plane) of the main, lowermost fracture as the only loading. The fluid overpressure used is 5 MPa, which is similar to the in situ tensile strength of most solid rocks (Haimson and Rummel, 1982; Schultz, 1995; Amadei and Stephansson, 1997). Most fluid transport in a fractured reservoir is through fluid-driven fractures, many of which have the potential of becoming non-stratabound and thus contributing significantly to the fluid transport in the reservoir. The clear dominating trends of the fractures (Fig. 4) indicate that they are primarily of tectonic origin and formed at depth, rather than related to an overall tensile stress generated by erosion and uplift of the area within which they are located. Most of the fractures are extension fractures. If they formed at depths greater than a few hundred metres, it follows from the Griffith Crack Theory that they cannot have formed as a result of tensile stresses and must, therefore, be the result of fluid overpressure (Gudmundsson et al., 2003), in agreement with the loading conditions in our model.

The numerical model was made using the boundary-element program BEASY. A description of the boundary-element method in general, and that of the BEASY program in particular, is provided by Brebbia and Dominguez (1992) and the BEASY homepage (www.beasy.com). Poisson's ratio is taken as 0.33 for all the layers, as is common for limestone (Bell, 2000; Nilsen and Palmstrøm, 2000). The stiffness of all the rock layers is taken as 50 GPa, a typical average laboratory value for many carbonate rocks such as limestones (Bell, 2000; Nilsen and Palmstrøm, 2000). The contacts between layers and joints in the layers above the hydrofracture are modelled as internal springs with a stiffness of 6 MPa/m. Such a low stiffness is appropriate for a contact or a joint with a consolidated,

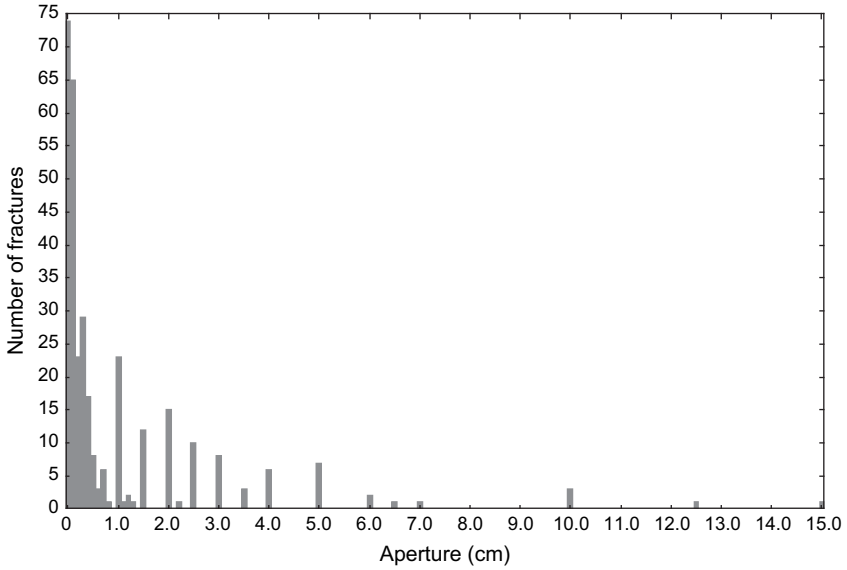

Fig. 10. Histogram of all measured fracture apertures in the Pizzicoli Quarry ($N = 324$).

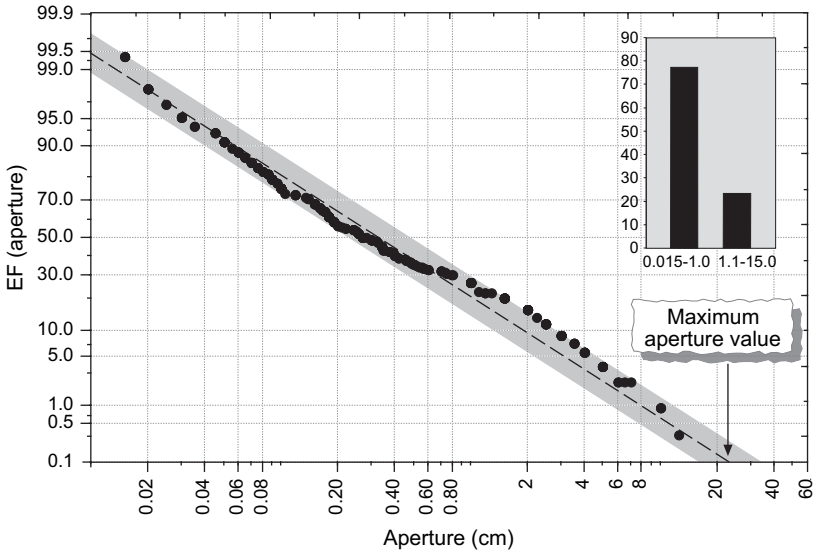

Fig. 11. Exceedence-frequency plot of all fracture-aperture measurements, with the aperture on a logarithmic scale and the frequency on a probability scale. The plot can be approximated as a straight line, indicating a log-normal distribution (with some artefacts). The extrapolated broken straight line gives the estimated maximum spacing value. The inset diagram shows the class limits and the frequency (%) of fracture apertures in the two main subpopulations.

elastic but soft infill, or a contact with a weak paleosol layer such as siliciclastic silt laminae, which are common in the quarry. For comparison, Young's moduli for weak mudrocks (e.g. marl) may be as low as 3 MPa (Bell, 2000).

The first results (Fig. 16) are for a model where the only loading is a 5 MPa overpressure in the large hydrofracture, and the vertical fractures in the layers above are modelled as internal springs. The model shows that the tensile stress induced by the propagating hydrofracture would be able to open many fractures in the layers above its tip. In particular, the fractures in the layer closest to the hydrofracture tip open up widely. Moreover, these fractures are linked by zones of high tensile stress to the fractures in the layer above. Since the tensile stresses in the zones combining the nearby fracture tips exceed several mega-pascals, it is likely that these fractures would combine to form an interconnected cluster. This follows because the in situ tensile strength of solid rocks is mostly in the range of 0.5–6 MPa (Haimson and Rummel, 1982; Schultz, 1995; Amadei and Stephansson, 1997). Thus, the tensile strength would commonly be exceeded in the zones between the nearby fracture tips, thereby forming small tensile fractures that would link the larger, open fractures. Similar results are obtained for shear-stress zones (not shown here) between the nearby tips of the main fractures, suggesting that some of the fractures might link through small transfer faults, as is commonly observed (Gudmundsson et al., 2003).

The opening of fractures in the layers above the hydrofracture reaches considerable distances from its tip. However, the local stress fields around the tips of the remote fractures are too small to

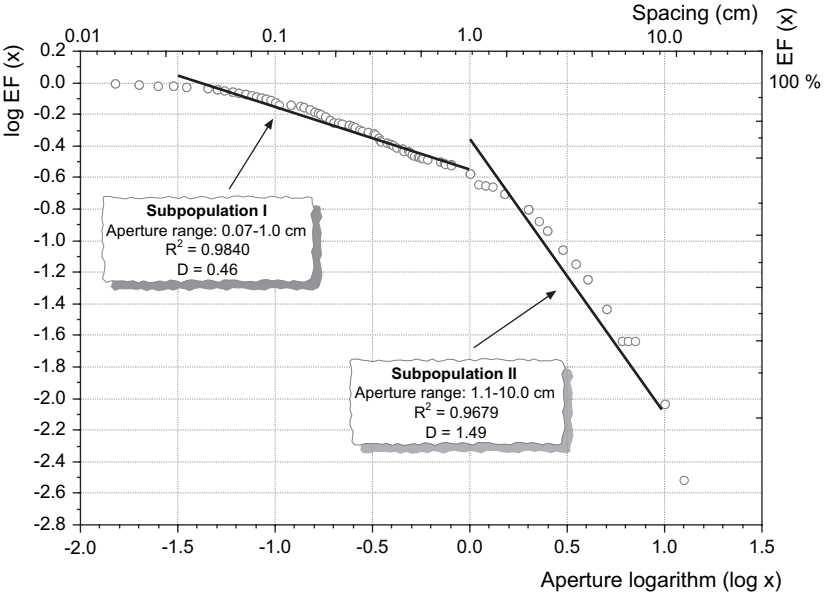

Fig. 12. Exceedence-frequency plot of the fracture-aperture data set, with both frequency and spacing on logarithmic scales. The graph can be approximated by two straight lines, of different dips, indicating two subpopulations of fracture aperture that are roughly power laws with different straight-line slopes D ("fractal dimensions").

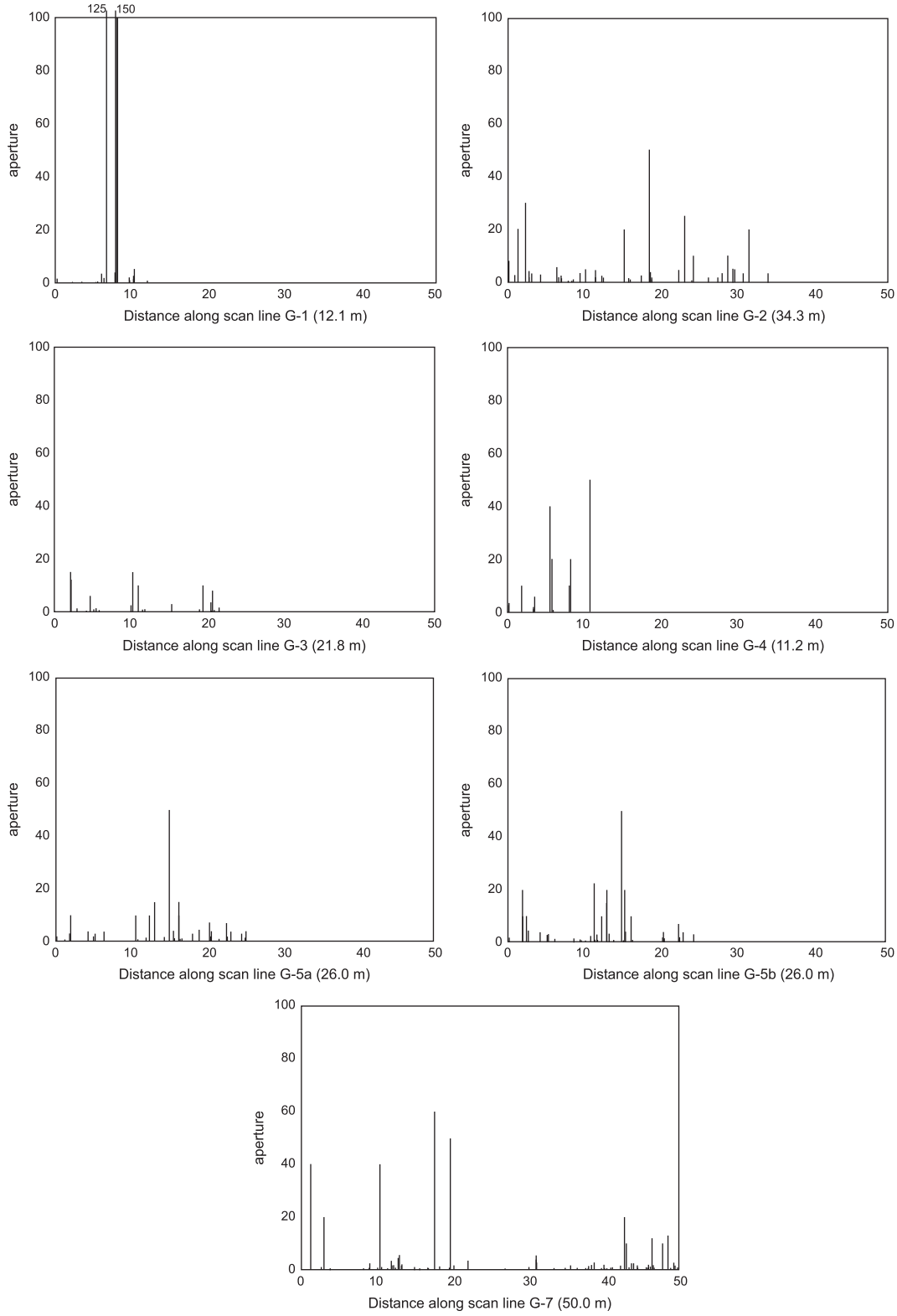

Fig. 13. Diagrams showing fracture aperture as a function of distance along seven scan lines. Aperture is given in millimetres and distance in metres.

form stress-zones between the nearby fracture tips. Thus, the remote fractures would be unlikely to link up to form clusters. It follows that their contribution to the overall permeability of this part of the reservoir would be negligible. Thus, in the present model, the only fractures likely to form a cluster, and therefore reach the percolation threshold, would be those within a comparatively narrow zone directly ahead of the main hydrofracture.

To check if the remote fractures could become part of an interconnected cluster, we also constructed a model where, in addition to the vertical fractures, the horizontal contacts are modelled as

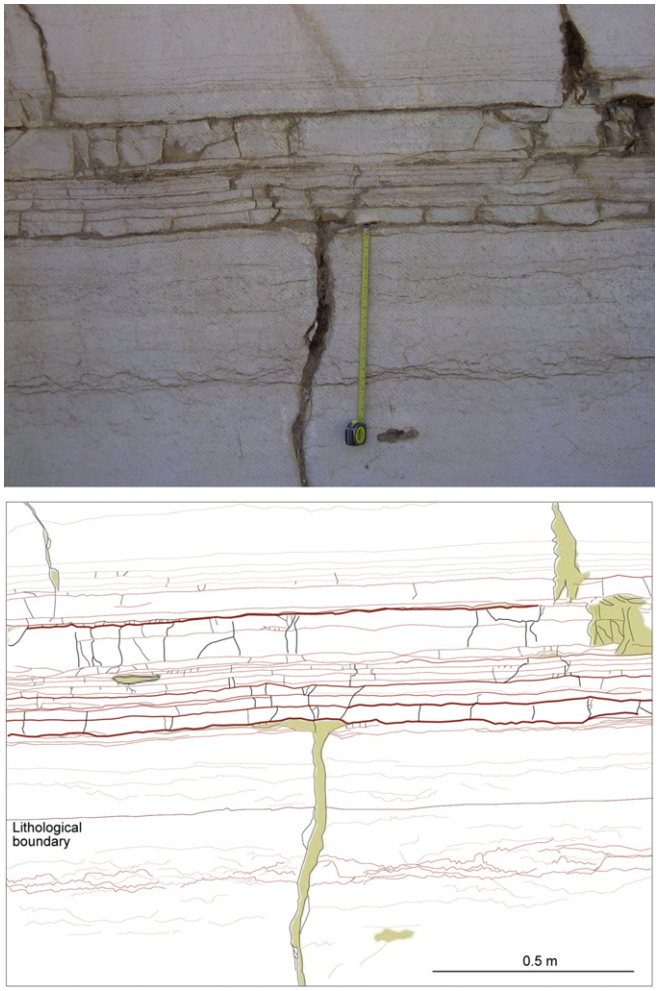

Fig. 14. Large fracture arrested at horizontal contact. This fracture, assumed to have been generated by fluid pressure, as well as the small fractures and contacts in the layers above its tip are used as a basis for the numerical models (Fig. 15).

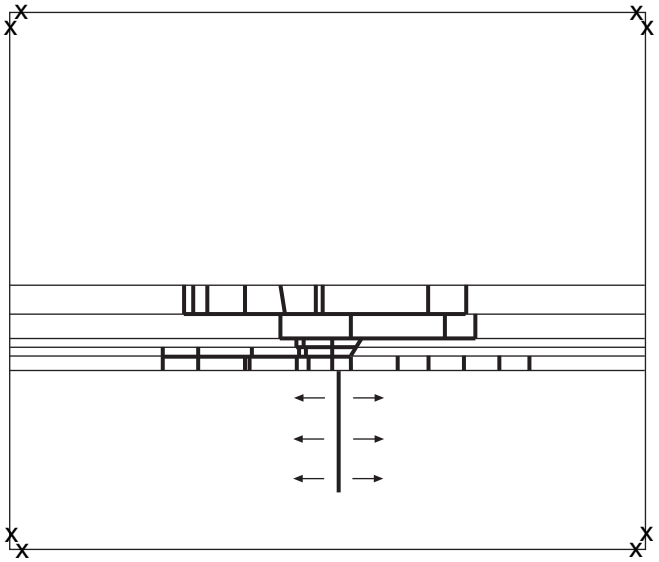

Fig. 15. The geometric configuration for the numerical models. All layers have Young's modulus (stiffness) of 50 GPa and Poisson's ratio 0.33. The contacts between layers, and joints in the layer above the hydrofracture, are modelled as internal springs with a stiffness of 6 MPa/m. The only loading is a fluid overpressure of 5 MPa/m in the lowermost (fluid-driven) large fracture.

internal springs (Fig. 17). Since the contacts between layers are weak discontinuities, thereby lowering the effective stiffness, the present model (and the part of the reservoir it represents) shows a greater deformation in response to the stresses induced by the hydrofracture when compared with the previous model (Fig. 16). However, the main effect as regards permeability is that the network of interconnected fractures becomes much larger (Fig. 17) than in the previous model (Fig. 16). This is primarily because parts of the horizontal contacts open up and become connected with several vertical fractures, many of which are remote.

As a consequence of a large part of the rock volume (a potential reservoir) being subject to significant deformation in the present model, the magnitudes of the hydrofracture-induced tensile stresses around the vertical fractures tend to be considerably less than in the previous model (cf. Figs. 16 and 17). However, so long as the tensile stress reaches or exceeds a few mega-pascals, the fracture network is likely to open up and form an interconnected cluster. Thus, in the present model (Fig. 17) the fluid flow is likely to occur in a larger part of the reservoir than in the previous model. By contrast, since the opening displacements (apertures) of the fractures ahead of the hydrofracture are more limited in this model (Fig. 17) than in the previous one (Fig. 16), the previous model is likely to give higher volumetric flow rates. This follows from the well-known cubic law for fluid flow in fractures (Lee and Farmer, 1993), which states that the volumetric flow rate is proportional to the third power of the fracture aperture. In both models, the basic results are that, for given loading conditions, the tensile stresses induced by the main hydrofracture are likely to results in the formation of an interconnected cluster of fractures which would contribute significantly to the permeability of this part of the carbonate reservoir.

5. Discussion

In this paper we discuss the effects of fractures, particularly their attitude and geometry, on the general permeability development in a carbonate reservoir. Cemented rocks such as those in the Pizzicoli Quarry are an excellent example of rocks of low intrinsic porosity and permeability but where interconnected fractures can subsequently generate considerable permeability (Figs. 14–17). How much fracture-related permeability develops in such rocks depends on many factors including rock lithology, dissolution, mechanical layering, and local stress fields.

While relationships between lithology and fracture density (frequency) are commonly reported (Aguilera, 1995), in the present study area there is no clear relationship between lithology and fracture density or distribution. One reason for the lack of correlation between lithology and fracture density is that the lithological boundaries between the main rock types, cemented wackestone and mudstone deposited in an inner shelf environment, are commonly unclear and difficult to determine. The only clear boundaries are those that occur between peritidal cycles and those that occur between the laminates of carbonate mudstone, the latter being divided by stylolites. A second reason is that the cementation not only makes it hard to distinguish any differences between lithologies, but also makes the different lithological layers behave in a similar mechanical manner. The third reason is that the mechanical contacts or discontinuities, which have clear effects on fracture density, do not coincide with lithological boundaries, except for the laminated carbonate mudstones. Thus, where the lithological boundaries can be seen, they are mostly not mechanical contacts and the fractures commonly propagate through them.

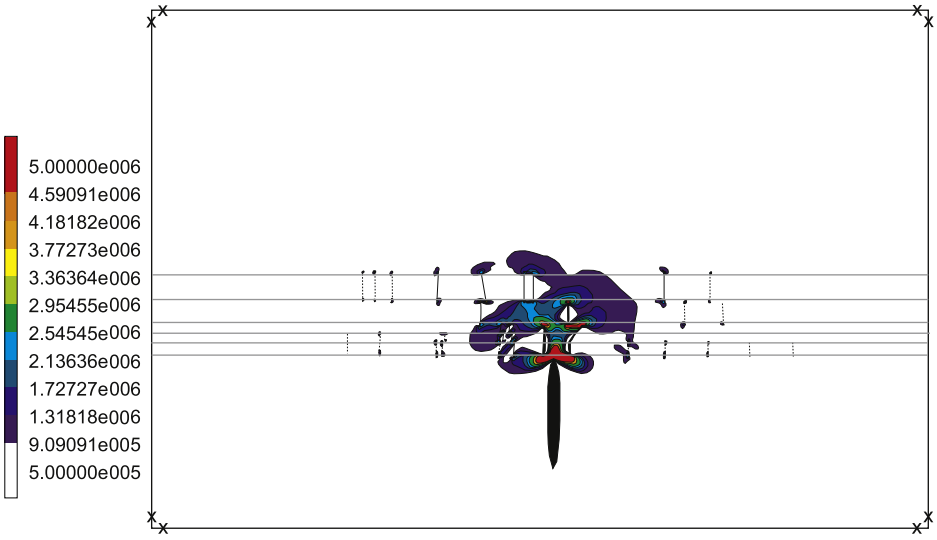

Fig. 16. Numerical model showing the magnitude of the maximum principal tensile stress, sigma 3, given in pascals as absolute values. In this model, the fractures in the thin layers are modelled as internal springs, but the horizontal contacts are strong ("welded").

Unlike lithological boundaries, mechanical layering has a great effect on fracture density and distribution. In the study area, one mechanical layer is separated from another by horizontal discontinuities which are either stylolite contacts or Intra-Cretaceous paleosols (of siliciclastic silt), and the layers vary in thickness from few centimetres (laminated carbonate mudstone) to 1–2 metres (peritidal cycles). The contacts are very variable in geometry and structure. Some are nodular-shaped with distinct stylolites where the teeth are visible (Fig. 18), whereas others are thin zones or multilayers (Fig. 2c), some of which have later been modified through karstification, seen as open cavities or, alternatively, cavities filled with red clay. Many fractures are arrested, offset or change attitude at these contacts.

There are, nevertheless, several examples where fractures in the vicinity of arrested fractures propagate through the same mechanical multilayered boundary (Fig. 19). One explanation might be that there was a change in the regional stress field in the time interval between the formation of the arrested and through-going fractures. Such an explanation could be feasible if the arrested and the non-arrested fractures had different attitudes. However, the three fractures in Fig. 19 all have similar attitudes. A more likely explanation for the existence of adjacent arrested and non-arrested fractures with similar attitude is that the layer through which they propagated functioned differently during the evolution of the rock. It is well known that an original multilayer, with weak or open contacts (thereby encouraging fracture arrest), may gradually become "welded" into a single mechanical layer with essentially uniform properties. Such a gradual homogenisation of the mechanical properties in a multilayer, and hence of its local stress field (stress homogenisation), is well known for layered rocks worldwide, in particular in volcanic areas, where many dykes (fluid-driven fractures) become arrested at contacts but which later-formed dykes could easily pass through (Gudmundsson, 2006; Gudmundsson and Brenner, 2006).

This brings us to the effects of local stresses on fracture propagation, fracture arrest and potential fracture-related permeability

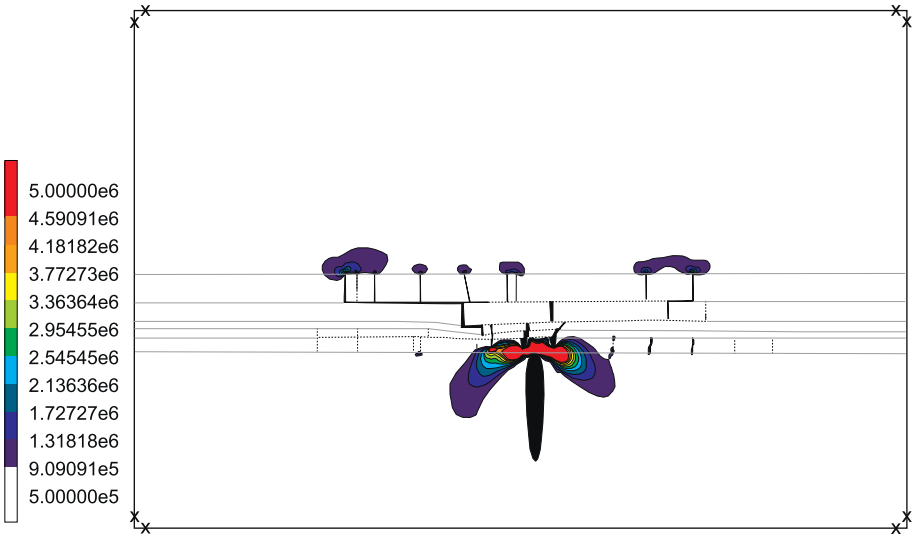

Fig. 17. Numerical model showing the magnitude of the maximum principal tensile stress, sigma 3, given in pascals as absolute values. In this model, both the fractures in the thin layers and some of the horizontal contacts are modelled as internal springs.

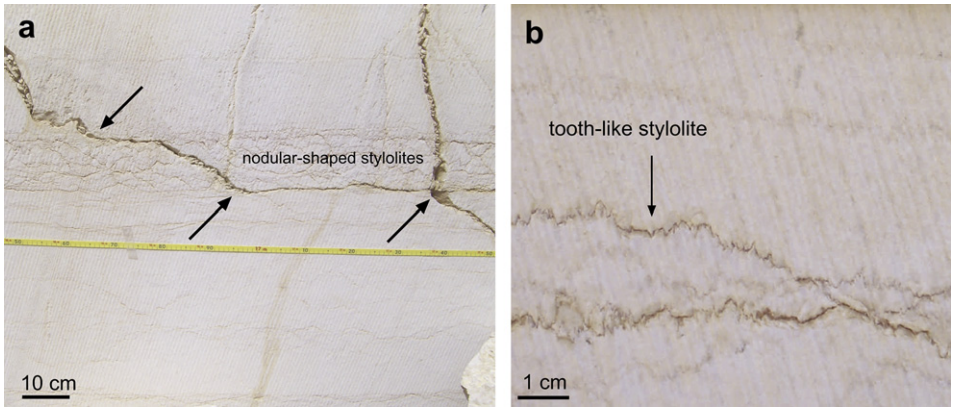

Fig. 18. (a) Nodular-shaped stylolites with tooth-like appearance affect fracture attitude which changes on meeting the nodular-stylolite layer (black arrows). (b) Close-up view of the tooth-like stylolites.

in layered rocks such as those in the study area. Our statistical data indicate that the fracture attitude is such that many of the fractures are likely to be interconnected (Fig. 4). Together with fracture size and location, it is the fracture attitude, largely a function of local stresses and their variation through time, that determines whether or not the fractures will intersect. Fracture intersections may occur if fractures are at significant angles to each other, which would usually mean two or more fracture sets. Parallel fractures will only allow fluid flow in one direction unless there is some primary permeability in the rock mass. The observed fractures, exposed in cemented wackestone and mudstone, are sub-vertical to vertical and strike in almost every direction. However, there is one main direction, E–W to ESE–WNW. There are also many fractures striking NNE–SSW which increases the likelihood of fractures intersecting. Within a rock mass of low to zero permeability, the fractures must be of a certain size (length or strike dimension and height or dip dimension) to interconnect rather than be isolated. While fracture dip dimensions could be easily measured in the quarry, limited exposure made it impossible to obtain large, systematic data sets on fracture strike dimensions.

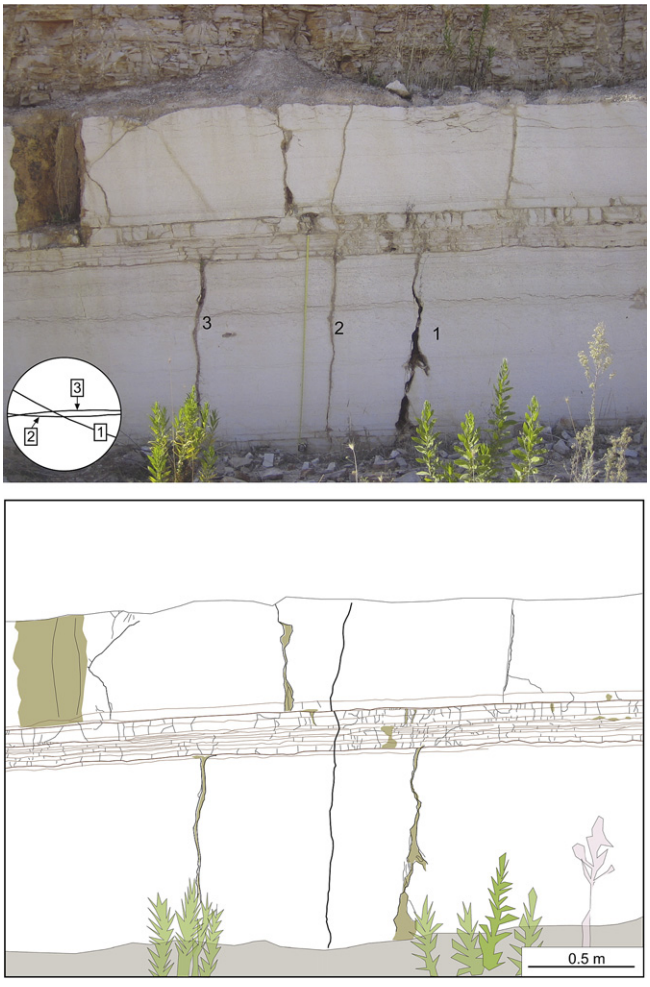

Fig. 19. Through-going (non-stratabound) fracture (2) with two adjacent arrested fractures (1 and 3). View NW.

Some of the fractures are filled with terra rossa from the sub-Miocene unconformity, indicating that they were open for some time after their formation. Later, during the Miocene, however, the fractures were modified through karstification. The stylolite horizons also experienced dissolution and were later filled with siliciclastic materials such as terra rossa from the Intra-Cretaceous paleosols; these are not laterally continuous.

As is indicated above, many fractures are arrested at the contacts between mechanical layers (Fig. 2c). In particular, where there are (laminated) multilayers, most fractures either become arrested or offset at the layer contacts (Fig. 9), indicating that it is normally difficult for fractures to propagate through such multilayers. More specifically, a multilayer, like many composite materials, possesses a high material toughness and a relatively large amount of energy is therefore required for a fracture to propagate through it (Hull and Clyne, 1996; Chawla, 1998; Hyer, 1998).

For many carbonate rocks, the formation of interconnected fracture clusters determines the fundamental process in forming and maintaining a comparatively high permeability. Given that fractures normally propagate through multilayers with great difficulty, provided the individual layers have different mechanical properties and that many fractures become arrested, we made several numerical models to analyse the formation of fracture clusters in such rocks (Fig. 14).

We used the exact geometry of one field example in the models (Fig. 14), so as to test if the stresses induced by the main fluid-driven fracture (hydrofracture) seen in the lower part of the field photograph would be high enough to generate an interconnected cluster. The results show that fluid-driven fractures (hydrofractures) with sufficient internal fluid overpressure (pressure in excess of the minimum compressive principal stress) may generate interconnected clusters in the layers above their tips. In particular, when the contacts in the multilayer are modelled as internal

springs, meaning that they were weak or open discontinuities at the time of hydrofracture propagation, the cluster of interconnected fractures and contacts becomes quite extensive (Fig. 17). We conclude that fluid overpressure (due to gas, oil, geothermal water, ground water) in major fractures can generate high-permeability fracture clusters within carbonate reservoirs.

6. Conclusions

- The fracture systems of Lower Cretaceous shallow-water carbonate platform limestone exposed in Pizzicoli Quarry are clustered with a mean C_v of 1.22 and a spatial distribution that is log-normal. On a log–log plot, however, it is noteworthy that the fracture spacings fall into three main groups or subpopulations, each of which is approximately a power law (a straight line on the log–log plot) and with a different straight-line slope. Most fractures, exposed in cemented wackestone and mudstone, are sub-vertical. Although they strike in almost every direction, the two main directions are E–W to ESE–WNW and NNE–SSW, suggesting that many fractures intersect.
- Fracture apertures also show a general log-normal size distribution, with a mean aperture of 1.01 cm and a median of 0.29 cm. However, on a log–log plot, most of the aperture measurements fall on one of two straight lines, suggesting that they belong to two subpopulations, each with a different straight-line slope.
- There is no clear correlation between lithology and fracture density or distribution. One reason for this lack of correlation is that boundaries between cemented wackestone and mudstone are mostly diffuse and difficult to determine. A second reason is that the cementation makes the different wackestone and mudstone mechanically similar. Consequently, the contacts of the mechanical layers, which have clear effects on fracture density, do not coincide with the (commonly obscure) wackestone and mudstone contacts.
- Many fractures are filled with terra rossa from the Sub-Miocene unconformity, suggesting that the fractures remained open for some time after their formation. The stylolite horizons are in some parts also filled with terra rossa, but these are not continuous laterally, again suggesting that some parts of the contacts acted, for a while, as open discontinuities.
- The field data also show that many fractures became arrested at the contacts between mechanical layers. To explore the conditions whereby arrested fractures induce stresses in the layers above their tips that encourage the formation of interconnected fracture clusters, we made several boundary-element models. We modelled the main arrested fractures as fluid driven (the fluid being gas, oil, water, or geothermal water) and calculated the effects of the induced stresses on the fractures in the layers above the hydrofracture tip.
- The results indicate that a hydrofracture is able to generate interconnected clusters in the layers above its tips, provided the fluid overpressure driving the fracture is sufficiently high (here 5 MPa). When in addition to open vertical fractures in the layers above the hydrofracture there are open or weak contacts between the layers in the multilayer above the tip, the cluster of interconnected fractures and contacts becomes quite extensive. Since overpressure is the total fluid pressure minus the normal stress on the fracture, it follows that fluid-driven opening of contacts and other discontinuities can theoretically occur at any crustal depth (Gudmundsson, 2006; Gudmundsson et al., 2003). We conclude that large hydrofractures can generate high-permeability fracture clusters within carbonate reservoirs.

Acknowledgements

This work was supported by the Norwegian Research Council Petromaks project no. 163316/S30 "Carbonate Reservoir Geomodels". We thank the Carbonate Research Group Members (International Research Institute of Stavanger, University of Bergen, Cambridge Carbonates Ltd, University of Bari and University of Göttingen) for support, Michael R. Talbot for the sedimentological contribution and for reading parts of the manuscript, Wojtek Nemec for the valuable input on statistics and Peppino Pizzicoli for giving permission to work in his quarry. We also thank Valerio Acocella, Paul Gillespie, Tom Blenkinsop, and an anonymous reviewer for the constructive and very helpful review comments.

References

Aguilera, R., 1995. Naturally Fractured Reservoirs. PennWell Books, Tulsa, Okla.
Amadei, B., Stephansson, O., 1997. Rock Stress and its Measurement. Chapman & Hall, London.
Anzidei, M., Baldi, P., Casula, G., Crespi, M., Riguzzi, F., 1996. Repeated GPS surveys across the Ionian Sea: evidence of crustal deformations. Geophysical Journal International 127, 257–267.
Bai, T., Pollard, D.D., Gao, H., 2000. Explanation for fracture spacing in layered materials. Nature 403, 753–756.
Bai, T.X., Pollard, D.D., 2001. Getting more for less: the unusual efficiency of fluid flow in fractures. Geophysical Research Letters 28, 65–68.
Becker, A., Gross, M.R., 1996. Mechanism for joint saturation in mechanically layered rocks: an example from southern Israel. Tectonophysics 257, 223–237.
Bell, F.G., 2000. Engineering Properties of Soils and Rocks, fourth ed. Blackwell, Oxford.
Bertotti, G., Casolari, E., Picotti, V., 1999. The Gargano Promontory: a Neogene contraction belt within the Adriatic Plate. Terra Nova 11, 168–173.
Bertotti, G., Picotti, V., Chilovi, C., Fantoni, R., Merlini, S., Mosconi, A., 2001. Neogene to Quaternary sedimentary basins in the south Adriatic (Central Mediterranean): foredeeps and lithospheric buckling. Tectonics 20, 771–787.
Billi, A., 2003. Solution slip and separations on strike-slip fault zones: theory and application to the Mattinata Fault, Italy. Journal of Structural Geology 25, 703–715.
Billi, A., Salvini, F., 2001. Fault-related solution cleavage in exposed carbonate reservoir rocks in the Southern Apennines, Italy. Journal of Petroleum Geology 24, 147–169.
Billi, A., Gambini, R., Nicolai, C., Storti, F., 2007. Neogene–Quaternary intraforeland transpression along a Mesozoic platform-basin margin: the Gargano fault system, Adria, Italy. Geosphere 3, 1–15.
Bosellini, A., 2002. Dinosaurs "re-write" the geodynamics of the eastern Mediterranean and the paleogeography of the Apulia Platform. Earth-Science Reviews 59, 211–234.
Bosellini, A., Neri, C., Luciani, V., 1993. Platform margin collapses and sequence stratigraphic organization of carbonate slopes: Cretaceous–Eocene, Gargano Promontory, Southern Italy. Terra Nova 5, 282–297.
Bosellini, A., Morsilli, M., Neri, C., 1999. Long-term event stratigraphy of the Apulia Platform margin (Upper Jurassic to Eocene, Gargano, southern Italy). Journal of Sedimentary Research 69, 1241–1252.
Brankman, C.M., Aydin, A., 2004. Uplift and contractional deformation along a segmented strike-slip fault system: the Gargano Promontory, southern Italy. Journal of Structural Geology 26, 807–824.
Brebbia, C.A., Dominguez, J., 1992. Boundary Elements: an Introductory Course. Computational Mechanics, Southampton.
Casolari, E., Negri, A., Picotti, V., Bertotti, G., 2000. Neogene stratigraphy and sedimentology of the Gargano Promontory (southern Italy). Eclogae Geologicae Helvetiae 93, 7–23.
Chawla, K.K., 1998. Composite Materials: Science and Engineering. Springer, New York.
Chilovi, C., De Feyter, A.J., Pompucci, A., 2000. Wrench zone reactivation in the Adriatic Block: the example of the Mattinata fault system (SE Italy). Bollettino della Societa Geologica Italiana 119, 3–8. 1 sheet.
Cox, D.R., Lewis, P.A.W., 1966. The Statistical Analysis of Series of Events. Chapman and Hall, London.
de Alteriis, G., 1995. Different foreland basins in Italy; examples from the central and southern Adriatic Sea. Tectonophysics 252, 349–373.
Doglioni, C., Mongelli, F., Pieri, P., 1994. The Puglia uplift (SE Italy): an anomaly in the foreland of the Apenninic subduction due to buckling of a thick continental lithosphere. Tectonics 13, 1309–1321.
Drummond, C.N., Wilkinson, B.H., 1996. Strata thickness frequencies and the prevalence of orderedness in stratigraphic sequences. Journal of Geology 104, 1–18.
Favali, P., Funiciello, R., Mattietti, G., Mele, G., Salvini, F., 1993. An active margin across the Adriatic Sea (Central Mediterranean-Sea). Tectonophysics 219, 109–117.

Gambini, R., Tozzi, M., 1996. Tertiary geodynamic evolution of the Southern Adria microplate. Terra Nova 8, 336–340.
Gillespie, P.A., Walsh, J.J., Watterson, J., Bonson, C.G., Manzocchi, T., 2001. Scaling relationships of joint and vein arrays from The Burren, Co. Clare, Ireland. Journal of Structural Geology 23, 183–201.
Gillespie, P.A., Johnston, J.D., Loriga, M.A., McCaffrey, K.J.W., Walsh, J.J., Watterson, J., 1999. Influence of layering on vein systematics in line samples. In: McCaffrey, K.J.W., Lonergan, L., Wilkinson, J.J. (Eds.), Fractures, Fluid Flow and Mineralization. Geological Society of London, Special Publication, vol. 155, pp. 35–56.
Graziano, R., 1999. The Early Cretaceous drowning unconformities of the Apulia carbonate platform (Gargano Promontory, southern Italy): local fingerprints of global palaeoceanographic events. Terra Nova 11, 245–250.
Graziano, R., 2000. The Aptian–Albian of the Apulia carbonate platform (Gargano Promontory, southern Italy): evidence of palaeoceanographic and tectonic controls on the stratigraphic architecture of the platform margin. Cretaceous Research 21, 107–126.
Gross, M.R., 1993. The origin and spacing of cross joints: examples from the Monterey Formation, Santa Barbara coastline, California. Journal of Structural Geology 15, 737–751.
Gudmundsson, A., 2006. How local stresses control magma-chamber ruptures, dyke injections, and eruptions in composite volcanoes. Earth-Science Reviews 79, 1–31.
Gudmundsson, A., Brenner, S.L., 2004. How mechanical layering affects local stresses, unrests, and eruptions of volcanoes. Geophysical Research Letters 31, 1–4.
Gudmundsson, A., Brenner, S.L., 2006. How local stress fields prevent volcanic eruptions. Journal of Volcanology and Geothermal Research 158, 257–268.
Gudmundsson, A., Gjesdal, O., Brenner, S.L., Fjeldskaar, I., 2003. Effects of linking up of discontinuities on fracture growth and groundwater transport. Hydrogeology Journal 11, 84–99.
Haimson, B.C., Rummel, F., 1982. Hydrofracturing stress measurements in the Iceland Research Drilling Project drill hole at Reydarfjordur, Iceland. Journal of Geophysical Research 87, 6631–6649.
Hobbs, D.W., 1967. The formation of tension joints in sedimentary rocks: an explanation. Geological Magazine 104, 550–556.
Huang, Q., Angelier, J., 1989. Fracture spacing and its relation to bed thickness. Geological Magazine 126, 355–362.
Hull, D., Clyne, T.W., 1996. An Introduction to Composite Materials. Cambridge University Press, Cambridge.
Hyer, M.W., 1998. Stress Analysis of Fiber-reinforced Composite Materials. McGraw-Hill, New York.
Karcz, Z., Scholz, C.H., 2003. The fractal geometry of some stylolites from the Calcare Massiccio Formation, Italy. Journal of Structural Geology 25, 1301–1316.
Laubach, S.E., Gale, J.F.W., 2006. Obtaining fracture information for low-permeability (tight) gas sandstones from sidewall cores. Journal of Petroleum Geology 29, 147–158.
Lee, C.H., Farmer, I., 1993. Fluid Flow in Discontinuous Rocks. Chapman & Hall, London.
Li, Y.P., Yang, C.H., 2007. On fracture saturation in layered rocks. International Journal of Rock Mechanics and Mining Sciences 44, 936–941.
Morsilli, M., Bosellini, A., 1997. Carbonate facies zonation of the upper Jurassic Lower Cretaceous Apulia platform margin (Gargano Promontory, Southern Italy). Rivista Italiana Di Paleontologia E Stratigrafia 103, 193–205.
Narr, W., Suppe, J., 1991. Joint spacing in sedimentary rocks. Journal of Structural Geology 13, 1037–1048.
Nickelsen, R.P., 1972. Attributes of rock cleavage in some mudstones and limestones of the Valley and Ridge Province, Pennsylvania. Pennsylvania Academy of Science 46, 107–112.
Nilsen, B., Palmstrøm, A., 2000. Engineering Geology and Rock Engineering. Norwegian Group for Rock Mechanics, Oslo.
Odling, N.E., Gillespie, P., Bourgine, B., Castaing, C., Chiles, J.P., Christensen, N.P., Fillion, E., Genter, A., Olsen, C., Thrane, L., Trice, R., Aarseth, E., Walsh, J.J., Watterson, J., 1999. Variations in fracture system geometry and their implications for fluid flow in fractured hydrocarbon reservoirs. Petroleum Geoscience 5, 373–384.
Odonne, F., Lezin, C., Massonnat, G., Escadeillas, G., 2007. The relationship between joint aperture, spacing distribution, vertical dimension and carbonate stratification: an example from the Kimmeridgian limestones of Pointe-du-Chay (France). Journal of Structural Geology 29, 746–758.
Ortega, O.J., Marrett, R.A., Laubach, S.E., 2006. A scale-independent approach to fracture intensity and average spacing measurement. AAPG Bulletin 90, 193–208.
Patacca, E., Scandone, P., 2004. The 1627 Gargano earthquake (Southern Italy): identification and characterization of the causative fault. Journal of Seismology 8, 259–273.
Pratt, B.R., James, N.P., Cowan, C.A., 1992. Peritidal Carbonates. Geological Association of Canada, St. Johns, NF.
Price, N.J., 1966. Fault and Joint Development in Brittle and Semi-brittle Rock. Pergamon Press, Oxford.
Priest, S.D., 1993. Discontinuity Analysis for Rock Engineering. Chapman & Hall.
Rives, T., Razack, M., Petit, J.P., Rawnsley, K.D., 1992. Joint spacing: analog and numerical simulations. Journal of Structural Geology 14, 925–937.
Salvini, F., Billi, A., Wise, D.U., 1999. Strike-slip fault-propagation cleavage in carbonate rocks: the Mattinata Fault Zone, Southern Apennines, Italy. Journal of Structural Geology 21, 1731–1749.
Schultz, R.A., 1995. Limits on strength and deformation properties of jointed basaltic rock masses. Rock Mechanics and Rock Engineering 28, 1–15.
Soudet, H.J., Sorriaux, P., Rolando, J.P., 1994. Relationship between fractures and karstification – the oil-bearing Paleokarst of Rospo Mare (Italy). Bulletin Des Centres De Recherches Exploration-Production Elf Aquitaine 18, 257–297.
Spalluto, L., 2004. The Gargano Promontory: Geological Framework, Stratigraphy of Mesozoic Carbonate Units and Tectonic Setting. Unpublished Ph.D. thesis, Universita Degli Studi di Bari.
Statsoft, 2007. Statistica: Data Analysis Software System, Version 7. www.statsoft.com.
Stauffer, D., Aharony, A., 1994. Introduction to Percolation Theory, second ed. Taylor and Francis, London.
Stow, D.A.V., 2005. Sedimentary Rocks in the Field: a Colour Guide. Manson Publ., London.
Tondi, E., Piccardi, L., Cacon, S., Kontny, B., Cello, G., 2005. Structural and time constraints for dextral shear along the seismogenic Mattinata Fault (Gargano, southern Italy). Journal of Geodynamics 40, 134–152.
Van der Pluijm, B.A., Marshak, S., 2004. Earth Structure, second ed. W.W. Norton & Company, New York.
Vartdal, M., 2006. A Sedimentological Study of the Apricena Calcarenite (Miocene), The Gargano Peninsula, Italy. Unpublished M.Sc. Thesis, 96 pp. (in Norwegian).
Wennberg, O.P., Svana, T., Azizzadeh, M., Aqrawi, A.M.M., Brockbank, P., Lyslo, K.B., Ogilvie, S., 2006. Fracture intensity vs. mechanical stratigraphy in platform top carbonates: the Aquitanian of the Asmari Formation, Khaviz Anticline, Zagros, SW Iran. Petroleum Geoscience 12, 235–245.
Wu, H., Pollard, D.D., 1995. An experimental study of the relationship between joint spacing and layer thickness. Journal of Structural Geology 17, 887–905.